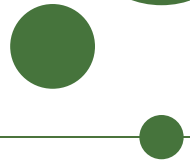


UNIVERSITY OF COPENHAGEN
FACULTY OF SCIENCE



PhD Dissertation

Michael. J. Larson

A Search for Tau Neutrino Appearance with IceCube-DeepCore

Advisor: Dr. D. Jason Koskinen

Handed in: March 13, 2018

Contents

1	Introduction	15
1.1	The History of the Neutrino	15
1.2	History of Cosmic Rays	16
1.3	Atmospheric Neutrinos	17
1.4	The Standard Model	18
1.5	Methods of Detection	22
2	Neutrino Oscillations	26
2.1	Oscillation Theory and the PMNS Matrix	26
2.2	Experimental Constraints on Neutrino Oscillations	29
2.3	Unitarity and Sterile Neutrinos	32
3	The IceCube Detector	38
3.1	The DOM: The Basic Unit of IceCube	38
3.2	The Geometry of the Detector	41
3.3	The Bulk Ice Model	46
3.4	The Hole Ice	47
4	Simulation of the IceCube-DeepCore Detector	49
4.1	Monte Carlo Generators	49
4.2	Propagation of the Particles and Light	53
4.3	Simulating the Detector Electronics	54
5	Updates to the Noise Simulation	57
5.1	A Summary of Previous Fits	57
5.2	Limitations and Disagreement with Previous Fits	58
5.3	Low-dt Noise from Vuvuzela	59
5.4	Updating the Fitting Code	60
5.5	Results of New Noise Fits	65
6	Low-Energy Muon Simulation	70
6.1	CORSIKA Generation In DeepCore	70
6.2	MuonGun for DeepCore	71
6.3	Simulation Efficiency with KDE Prescales	73
7	GRECO: An Event Selection at the Limits of DeepCore	76
7.1	Hit Cleaning	76
7.2	Level 1: The DeepCoreFilter	78
7.3	Low-En Level 3 Cuts	79
7.4	GRECO Level 4 Cuts	81
7.5	GRECO Level 5 Cuts	86

7.6	GRECO Level 6 Cuts	91
7.7	GRECO Level 7: Final Level	97
7.8	Calibration Discoveries with GRECO	100
7.9	The Properties of the GRECO Event Selection	112
8	A Search for Tau Neutrinos from Oscillations	114
8.1	Expectations from Monte Carlo	114
8.2	Parametrizing the Tau Neutrino Appearance	115
8.3	Systematics Considerations	117
8.4	The Method of Maximum Likelihood	123
8.5	Expected Sensitivity to Appearance	127
8.6	Fitting Data	133
8.7	Results from the Search for Appearance	134
8.8	Complementary Measurements from This Analysis	138
8.9	New Constraints on Detector Systematics	139

List of Figures

1.1	The number of active neutrinos as measured by ALEPH, DELPHI, L3, and OPAL. The data from the four experiments strongly favors only three neutrinos coupling to the Z boson. Image taken from [ALEPH-3Nu].	16
1.2	The cosmic ray spectrum covers many orders of magnitude and has been verified by many experiments to high precision. The various features are thought to be caused by multiple sources at different scales. Image taken from [2]	18
1.3	The expected neutrino flux at Kamioka mine, Japan (Super-Kamiokande, top left), Ino Peak, India (India-based Neutrino Observatory, top right), the South Pole (IceCube, bottom left), and Pyhasalmi mine, Finland (EMMA experiment, bottom right) as a function of energy. Note that the neutrino and anti-neutrino fluxes are characterized separately. The differences in the flux at each site is due to differences in the Earth's magnetic field and temperature profile. Figure taken from [Honda-2015].	19
1.4	The expected flux of 3.2 GeV neutrinos at Kamioka mine, Japan; Ino Peak, India; the South Pole; and Pyhasalmi mine, Finland as a function of zenith angle. A value of $\cos \theta_Z = -1$ indicates neutrinos passing through the entire Earth and entering the detector from below while a value of $\cos \theta_Z = +1$ indicates neutrinos interacting in the atmosphere directly above the detector. The differences in the flux at each site is due to differences in the Earth's magnetic field and temperature profile. Figure taken from [Honda-2015].	19
1.5	The Standard Model of particle physics is made up of charged and uncharged leptons, quarks, and the various bosons. Image taken from [StandardModel-Image]	20
1.6	Feynman diagrams showing the interaction vertex of the neutrino with the W and Z boson.	20
1.7	The relative contributions to the cross section for ν (left) and $\bar{\nu}$ (right). The QE events dominate below 1 GeV while the DIS events dominate above 10 GeV. Note the different scales for the neutrino and antineutrinos. Images taken from [Formaggio-Xsec]	21
1.8	A Feynman diagram showing an example of a CC neutrino DIS interaction. An incident muon neutrino interacts with a quark inside of a proton. The result is a hadronic shower as well as a charged muon. Diagram taken from [Formaggio-Xsec]	22
1.9	An example of the energy loss ($\frac{-dE}{dx}$) calculated for muons incident on copper. Note the radiative losses due to bremsstrahlung, pair production, and photonuclear interactions above 1 TeV. Note also the labeled minimum demonstrating the energy of a minimum ionizing particle. Image taken from [2].	24

2.1	The first atmospheric neutrino oscillation measurements from the Super-K experiment. (a) The ν_e -like events show no shape in L/E, as expected from a lack of neutrino oscillations. The ν_μ -like interactions, however, show a clear drop, indicating the presence of oscillation effects. (b) Using the two neutrino approximation, Super-K produced contours of the best-fit oscillation parameters for $\nu_\mu \rightarrow \nu_\tau$ oscillations. Both figures from [SuperK-Oscillations]	31
2.2	The global best-fit values for the three flavor neutrino oscillation fits as of November 2017. The first column shows results assuming the normal ordering while the second column shows the results for the inverted ordering. Image taken from [NuFit.org]	32
2.3	Expectations (a) and results (b) of searches for sterile neutrinos in the neutral current interactions. (a) Effect of three hypothetical sterile neutrinos on the measurements of the MINOS detector [MINOS-SterileNC-2016]. "ND" and "FD" refer to the near and far detector of MINOS respectively. The sterile neutrinos have a small effect on the main oscillation minimum in the charged current channel, but up to 15% of the neutral current events are lost. (b) The results of the NO ν A search for sterile neutrinos using neutral current events. The limits are interpreted in terms of the 4x4 PMNS mixing elements in order to compare to searches with charged current interactions in Super-Kamiokande [SuperK-Steriles2015] and IceCube [10].	33
2.4	The results of the tests using 2.25 (solid) and 2.26 (dotted). A smaller value on the x-axis indicates a tighter constraint on observed unitarity of the 3x3 mixing matrix. Tests involving only muon or electron flavors show significantly tighter constraints than those including the tau flavor. Image taken from [Parke-Unitarity]	35
2.5	The constraints from a global fit to neutrino oscillation data[Parke-Unitarity] with an assumption of unitarity (black dotted) or no assumption of unitarity (red solid). The first two rows show little change from the unitarity assumption, indicating strong constraints from direct measurements. The elements of the third row, related to the ν_τ , show much larger changes, indicating that constraints are obtained from indirect oscillation measurements.	36
3.1	The IceCube DOM contains multiple components, including the PMT itself as well as various electronics necessary for semi-autonomous operation.	38
3.2	Afterpulsing calibration measurements performed in the lab. LEDs with known brightness were flashed to test for offtime response of the IceCube PMT. Clear dips, corresponding to detected charge, are visible. Drop (a) corresponds to the initial LED flash while (b), (c), and (d) show prominent afterpulsing peaks. Image taken from [IceCube-PMT].	39
3.3	Examples of the ATWD (top) and FADC (bottom) waveforms output from an IceCube PMT. Taken from [15]	40
3.4	A histogram of the time between subsequent hits on DOM 15 of string 27. Hitspool data, specialized data collected with no trigger applied, is shown in blue. The "correlated" (non-Poissonian) and "uncorrelated" (Poissonian) features are shown in red and black respectively. The location of a large afterpulsing peak is shown in yellow. Note that the features included are not to scale. Image taken from [15].	41

3.5	The IceCube Neutrino Observatory. Three separate subdetectors are shown: IceTop, a cosmic ray air shower detector; IceCube, an array designed to search for astrophysical neutrinos; and DeepCore, a dense subarray optimized for atmospheric oscillation physics measurements. The detector was deployed over multiple years. Strings deployed in the same year are shown with identical colors at the surface.	42
3.6	A comparison of the standard IceCube string (right) to the DeepCore string (left). The IceCube string uses DOMs spaced 17 m apart while DeepCore divides the DOMs into a fiducial (bottom) and veto plug (top). The dust concentration is shown in red. The concentration of dust in the ice affects the scattering and absorption of the glacial ice.	43
3.7	Examples of event topologies above 1 TeV using the full IceCube array. Event views shown in (a) and (b) are from actual events discovered by the IceCube detector [IceCube-AstroNu]. Images taken from [17]. (a) ν_e CC and ν NC show similar behavior from electromagnetic and hadronic interactions, which result in a shower of particles that quickly scatter in the ice. Cherenkov emission from these events appears roughly spherical in the detector. These events are known as "cascades". (b) ν_μ CC events begin with a hadronic interaction, then produce Cherenkov light from the outgoing muon. Above 1 TeV, the track of the outgoing muon becomes clearly visible. (c) Above 10 TeV, the tau lepton from a ν_τ CC may travel a significant distance before decaying. This results in two well-separated cascades in the detector, a tell-tale signature of ν_τ CC interactions.	44
3.8	The layout of the DeepCore detector. DeepCore is installed at the bottom of the IceCube detector in the clearest ice. A subset of DOMs were also deployed above DeepCore to improve muon identification of very-downgoing events.	45
3.9	A selection of 50 GeV simulated events in DeepCore taken from [17]. Unlike the event topologies at high energies, DeepCore events do not show distinct event types.	45
3.10	The data from the dust loggers deployed in various drill holes in IceCube during deployment. Data from individual holes has been offset in the y direction for clarity. Larger relative values of the "Optical Signal" represent more scattering in the ice while smaller values indicate clearer ice. The "dust layer" is visible in all drill holes around 2000 m. Deepcore DOMs are deployed below this layer. Image taken from [IceCube-DustLogger-Raw]. . .	46
3.11	The absorption and effective scattering properties of the ice as fit to flasher data. Two models are shown representing different generations of ice models used for simulation. The "Mie" model does not include anisotropy while the "Lea" model does. Figure from [6].	47
3.12	The effect of the anisotropy on the light output from a flasher on string 63. Measurements (points) are shown for receiving DOMs at three distances: at 125 m (red), at 217 m (blue), and at 250 m (green). A line is included to show the expected effect of anisotropy at each distance. The y-axis shows the ratio of a simulation of the same flasher without including anisotropy to data. A modulation is observed as a function of direction in the x-y plane. .	47

4.1	Average energy losses ($\frac{-dE}{dx}$) for a muon in ice. At very low energies, ionization losses dominate. Above approximately 1 TeV, pair production and photonuclear effects become more important. Image taken from [Dima-MMC]	53
4.2	Examples of the angular acceptance models used by IceCube. The relative sensitivity as a function of arrival direction is shown with $\cos(\eta)=-1$ indicating the back of the PMT and $\cos(\eta)=1$ the face. The variation of the acceptance model used for this search is shown using by varying two parameters in the model. The 'p' parameter primarily controls the acceptance at the side of the DOM while the 'p2' parameter controls the acceptance from the forward region. A second model, H2, is also shown.	55
4.3	The SPE template used in Monte Carlo simulation. The gaussian (red, dash-dot) and exponential (blue, dashed) parts of the full model (black) are shown. The SPE template is used as a sampling distribution for each incident photon in order to determine the observed charge. The SPE template is used for all DOMs.	56
5.1	Two examples of the original calibration work for the Vuvuzela model. The distribution of the time ("dt") between hits is shown. In black, untriggered detector data is shown. In red, a purely Poissonian noise model is shown. An afterpulsing peak is visible at 10^{-5} s. The Vuvuzela model is shown in blue. The Vuvuzela model shows improved agreement with data at all timescales.	58
5.2	The rates of events in DeepCore as a function of the number of hit DOMs in a cleaned hit series. The data, shown in black, consists of two components: the accidental triggers (red) and the atmospheric muons (blue). Accidental triggers produced using the Vuvuzela noise model reproduce most of the rate of events below 10 hit DOMs, although a rate disagreement remains. Image from [1].	59
5.3	The number of hit DOMs satisfying the (a) HLC and (b) SLC criteria described in Section 3.1.2. The distribution from 8 hours of data (black) is shown compared to a sample of CORSIKA muons at low-energy ($600 \text{ GeV} \leq E_{\text{primary}} \leq 100 \text{ TeV}$) and high energy ($100 \text{ TeV} \leq E_{\text{primary}} \leq 100 \text{ EeV}$). The addition of the low-dt extension to Vuvuzela improves the agreement between data and simulation in both HLC and SLC distributions.	60
5.4	The total amount of charge on DOMs satisfying the (a) HLC and (b) SLC criteria described in Section 3.1.2. The distribution from 8 hours of data (black) is shown compared to a sample of CORSIKA muons at low-energy ($600 \text{ GeV} \leq E_{\text{primary}} \leq 100 \text{ TeV}$) and high energy ($100 \text{ TeV} \leq E_{\text{primary}} \leq 100 \text{ EeV}$). Unlike in Figure 5.3, the charge distributions using the low-dt extension to Vuvuzela shows large disagreements with data. This is most visible in the SLC charge distribution.	61
5.5	The effect of changing the noise distribution parameters on the charge. Note the scale of the y-axis, which is scaled in order to emphasize the effect. Here, the gaussian mean is shifted from "5" (100 microseconds) to "3" (1 microsecond). All other parameters are held constant. By moving the correlated noise distribution to shorter timescales, more of distribution falls into one FADC bin, increasing the charge output for each launch.	61
5.6	A schematic diagram of the process used in the Vuvuzela V2 calibration fit.	62

5.7	Two examples of the new calibration fits for the Vuvuzela V2 model. The distribution of the time ("dt") between hits is shown on top. The distribution of charge is shown on the bottom. Note the y-axis of the charge distribution. In black, untriggered detector data is shown. The Vuvuzela V2 model is shown in blue. The new fits show good agreement in both time and charge distributions.	63
5.8	The distributions of each new fit parameter in the Vuvuzela V2 model. The colorbar scale shows the number of DOMs in each bin. The effects of fit bounds are visible in most distributions except for the thermal noise rate and the width of the log-normal distribution describing the non-Poissonian noise.	67
5.9	The distributions of each new fit parameter in the Vuvuzela V2 model as a function of the string and DOM number. Note that the top of the detector is at the bottom of this plot. No parameter appears to be correlated with depth. DOMs on string 25 are missing from the dataset. In addition, DOMs which are disabled due to malfunction are also unavailable.	68
5.10	The log-likelihood as a function of string and DOM number for the Vuvuzela V2 fits. Note that DOM 1 is at the top of the detector and DOM 60 at the bottom. The likelihood value was expected to be independent of depth, but shows some structure. These structures are correlated with both the ice model and the muon flux.	69
6.1	The distribution of CORSIKA muon energies at the MuonGun generation surface using GRECO Level 5 muon events. Very few events trigger are seen below 160 GeV and less than 5% of events occur beyond 500 GeV. These two energies set the bounds for the MuonGun generation. MuonGun simulation has also been produced and tested above 500 GeV, but no simulated events survived to final level in GRECO.	72
6.2	The generated spectrum from MuonGun in energy and zenith angle compared to the events reaching the final level of the GRECO event selection. Both distributions have been normalized to 1. The majority of events produced by MuonGun are downgoing and low energy. These events do not reach final level.	73
6.3	The generated spectrum from MuonGun in energy and azimuthal angle compared to the events reaching the final level of the GRECO event selection. Both distributions have been normalized to 1. Events in the final level sample are strongly biased in azimuth due to the geometry of the detector.	74
7.1	An illustration of the LC, SeededRT, and time window cleaning methods. (Left) All SLC pulses are removed while all HLC pulses are retained. (Middle) Pulses are removed based on time and distance from nearby HLC DOMs, allowing some SLC pulses to be accepted. (Right) Pulses are removed using the time relative to either the trigger (STW) or the maximum pulse density in time (DTW).	77
7.2	The distribution of effective particle speeds used by the DeepCoreFilter to identify and reject muons. Because muons interact first outside of DeepCore, a large peak is visible at speeds around 0.3 m/ns, the speed of light. Figure from [16].	79
7.3	The FirstHit Z position	82
7.4	Number of Hits Above Z=-200	82

7.5	QR6 and C2QR6	83
7.6	Tensor-of-Inertia Eigenvalue Ratio	83
7.7	The improvedLineFit Speed	84
7.8	The L4 BDT Score	85
7.9	Time to 75% Charge	87
7.10	A schematic diagram showing the regions of the VICH algorithm. VICH returns the number of hit DOMs in the shaded region, corresponding to the pulses that are both causally connected with the trigger and entering DeepCore.	87
7.11	Veto Identified Causal Hits	88
7.12	First Hit ρ Position	88
7.13	Quartile Distance	88
7.14	Quartile Z-Travel	89
7.15	SPE Reconstruction Zenith Angles	89
7.16	The L5 BDT Score	91
7.17	Fill-Ratio	93
7.18	The NChannel Distribution	94
7.19	CorridorCut Distribution	95
7.20	Example of Corridors into DeepCore	96
7.21	The FiniteReco Containment Cuts	96
7.22	Diagram Describing the FiniteReco Method	97
7.23	The effect of the data SPE correction applied in 2015	103
7.24	A comparison if the old and new SPE templates for simulation	104
7.25	A comparison of the charge extraction in data and simulation at GRECO L7. Both the time and charge are shown for individual pulses on all DOMs. The time is measured relative to the largest pulse observed on each DOM during an event. The data and simulation histograms are independently normalized to 1.0. While the two show broad agreement, notable differences occur at low charge.	105
7.26	The reconstructed Z position plotted against the reconstructed distance from string 36. The L7 cuts from GRECO have been removed for this plot. The colorbars in both plots have been normalized to be identical. The data and simulation show reasonable agreement except for two points in the data, near $\rho_{36} = 75$ at depths of -310 and -490.	106
7.27	The reconstructed X position and Y position of events in the detector. The L7 cuts from GRECO have been removed for this plot. The colorbars in both plots have been normalized to be identical. Once again, reasonable agreement is observed in most regions, although data events have a clear excess near $x=110$ m, $y=-60$ m. This position corresponds to string 83.	107
7.28	The RMS of the charges showing the events with flaring DOMs	108
7.29	The reconstructed Z position using PegLeg. The GRECO L7 cuts have not been applied in order to show discrepancies below the detector. Noticeable disagreement is seen below the detector at a depth of -500 m. Additional disagreements are also visible at the top of DeepCore, a region dominated by atmospheric muons.	109
7.30	The NuGen and GENIE true energy spectra at final level	109
7.31	The NuGen and GENIE interaction depths at final level	110
7.32	The reconstructed azimuthal direction from Pegleg	111

7.33	The true neutrino energy and zenith of the GRECO sample at final level. The sample shows an asymmetry between upgoing ($\cos(\theta) < 0$) and downgoing ($\cos(\theta) > 0$) event rates in the neutrinos due to selection bias. The sample has a long tail of events at both high and low energies. Using the NuFit 2.2 oscillation parameters and the flux model from Honda, the ν_τ events are observed in the very upgoing region around $10^{1.4} = 25$ GeV.	112
7.34	The reconstructed energy and zenith of the GRECO sample at final level. Events in data reconstruct to both relatively high energies ($E_R > 100$ GeV) and very low energies ($E_R \approx 2$ GeV). Using the NuFit 2.2 oscillation parameters and the flux model from Honda, the ν_τ events are observed in the very upgoing region around $10^{1.4} = 25$ GeV.	113
8.1	The sensitivity of this analysis in the (a) NC+CC and (b) CC-only channel. The top plot shows the Asimov expectation (black dotted line) and the Brazilian flag (green, yellow bands). The significances assuming Wilk's theorem (gray horizontal lines) and Feldman-Cousins (red horizontal lines) are also shown. The bottom plot shows the expected 1σ and 90% ranges for Wilks theorem and Feldman-Cousins compared to the most recent results from the OPERA and Super-Kamiokande analyses.	128
8.2	The test statistic distributions for 11 points in N_τ^{True} in the NC+CC fit. The assumption of 1 degree of freedom from Wilk's theorem is tested by looking at the location of $(\Delta\chi^2_{FS})_{90\%}$ for each point. The distribution calculated from Monte Carlo trials is narrower than that predicted by Wilk's theorem, indicating that a more complete treatment with the Feldman-Cousins procedure is necessary.	131
8.3	The value of each systematic with priors. The best-fit values are shown for each while the priors are shown by the yellow band. The CC and NC+CC fits are highly correlated, as expected, with very little difference in the systematics best-fit values. All values fit well within the expected 1σ ranges.	135
8.4	A comparison of the posterior expected from trials to the final data fit value for each parameter for the CC-only fit. The trials used to build the posterior distribution in each parameter assume baseline values for systematics, $N_\tau^{CC} = 1$, and Nu-Fit 2.2 values [NuFit_2.2]. The green vertical line shows the true injected value. The blue dotted line shows the best-fit value from data. The black bar shows the 1σ and 90% ranges calculated from the posterior distribution.	135
8.5	A comparison of the posterior expected from trials to the final data fit value for each parameter for the NC+CC fit. The trials used to build the posterior distribution in each parameter assume baseline values for systematics, $N_\tau^{NC+CC} = 1$, and Nu-Fit 2.2 values [NuFit_2.2]	136

List of Tables

1.1	The branching ratios for the decay of tau leptons. Two-thirds of the time, the tau lepton decays hadronically.	23
6.1	The simulation requirements needed for the production of the standard CORSIKA sets in IceCube. The number of events reaching final level of the appearance search (Section 7.6.3) are shown. CORSIKA simulations are computationally intensive, but inadequate for low energy analyses in IceCube.	71
6.2	The simulation requirements needed for the production of MuonGun simulation for DeepCore. The MuonGun simulation is nearly two orders of magnitude more efficient at producing statistics at final level in the appearance analysis.	72
6.3	The simulation requirements and number of events for each muon generation scheme. The use of the KDE prescale improves the simulation efficiency by a factor of 50x compared to the DeepCore MuonGun simulation method described in Section 6.1.	75
7.1	The event rates after the Level 3 cuts in GRECO. The total simulated rate is calculated using CORSIKA events and ignoring MuonGun. The data rate is estimated from a burn sample of 10 runs at Level 3. Rates are given in mHz.	81
7.2	The event rates after the Level 4 cuts in GRECO. The total simulated rate is calculated using CORSIKA events and ignoring MuonGun. The data rate is estimated from a burn sample of 30 runs at Level 4. Rates are given in mHz.	86
7.3	The event rates after the Level 5 cuts in GRECO. The total simulated rate is calculated using CORSIKA events and ignoring MuonGun. The data rate is estimated from a burn sample of 30 runs at Level 5. Rates are given in mHz.	92
7.4	The FiniteReco containment cut applied at GRECO Level 6	98
7.5	The event rates after the Level 6 cuts in GRECO. The total simulated rate is calculated using CORSIKA events and ignoring MuonGun. The data rate is estimated from a burn sample of 100 runs at Level 6. Rates are given in mHz.	99
7.6	The Pegleg containment cuts applied at Level 7	101
7.7	The 2D cuts applied to the time and energy variables at Level 7	102
7.8	The event rates at each cut level in the GRECO selection. Note that the MuonGun events are included in this table, but do not contribute to the total Monte Carlo expectation to prevent double-counting of muon events from the CORSIKA sample. All rates are given in millihertz.	112
8.1	The rates expected for each of the neutrino types in the Super-Kamiokande search for ν_τ appearance. Reproduced from.	117

8.2	Total χ^2 impact of each of the oscillation parameters. The atmospheric mixing parameters, Δm_{31}^2 and θ_{23} are the most important oscillation parameters for the GRECO selection. Of the remaining parameters, the CP-violating phase is the next most important.	118
8.3	Systematics sets used for the characterization of the signal neutrino events. While all listed sets have up to 30 years of effective livetime available, not all events are processed in each set.	119
8.4	Systematics sets used for the characterization of the atmospheric muon background.	120
8.5	Priors and allowed ranges for each systematic included in this analysis.	126
8.6	The best-fit systematics values for each nuisance parameter in the fit. The corresponding parameters for $N_\tau = 1$ (ie, the disappearance fit) are included for reference. The CC-only and NC+CC fits are highly correlated, as expected.	137

Updates to the Noise Simulation

5

The search for tau neutrinos is a search for rare particles near the detector threshold. Under these conditions, the search requires excellent understanding of threshold effects and detector behavior. In order to better model the detector, the noise simulation used in IceCube was updated with improved measurements after the discovery of disagreements in charge variables. This process is described in this chapter.

The chapter begins by describing the process used in previously to fit the Vuvuzela noise model for each DOM in Section 5. The limitations of the previous fitting process and the discovery of new disagreements is discussed in Sections 5.1 and 5.2 respectively. The new fitting procedure is then described in Section 5.3. New results of the fitting procedure are then discussed in Section 5.4.

5.1 A Summary of Previous Fits

Detector noise is a nuisance in most physics and astronomy experiments. PMT noise is assumed to be due to random emission from the photocathode and is affected by the gain of the PMT. Noise pulses from PMTs appear uniformly in time as a Poisson process.

The Poissonian noise model was used in the past in IceCube. With the introduction of the lower trigger threshold in DeepCore in 2010, however, it became clear that additional unsimulated sources of noise exist [1]. These additional hits appeared to occur in ‘bursts’ on a single PMT extending for up to a millisecond. Due to the time-correlations of these hits, the phenomenon was labeled *correlated noise*.

The Vuvuzela model, described briefly in Section 3.1.4, is now used to model both the Poissonian and non-Poissonian noise in IceCube. The empirical model consists of a Poisson process for electronic noise and radioactive decays and a correlated component modeled with a log-normal distribution. The model contains five free parameters per DOM. Ten minutes of untriggered data from the detector, dominated by noise hits, was used for calibration of the Vuvuzela parameters.

The Vuvuzela noise model is fit using the distributions of the time between subsequent hits, shown previously in Figure 3.4. Fits for each DOM were performed using the Pearson chi-squared test statistic between the data histogram, d , and the simulated histogram, m .

$$\chi^2 = \sum_i^{bins} \frac{(d_i - m_i)^2}{m_i} \quad (5.1)$$

The value of the χ^2 was minimized using a Metropolis-Hastings algorithm [2]. For each iteration of the algorithm, new parameters were selected and the response of the DOM was resimulated using PMTResponseSimulator and DOMLauncher. Each fit was computationally intensive, requiring between two and four CPU-weeks for each DOM. Due to the computationally requirements of the fits, the stopping condition was intentionally loosely defined, with a goodness-of-fit of 10% used.

Two examples from the original calibration work are shown in Figure 5.1. The Poissonian noise model used previously is shown for comparison. The Vuvuzela model more accurately reproduces the observed data across all timescales. Distributions of the number of hit

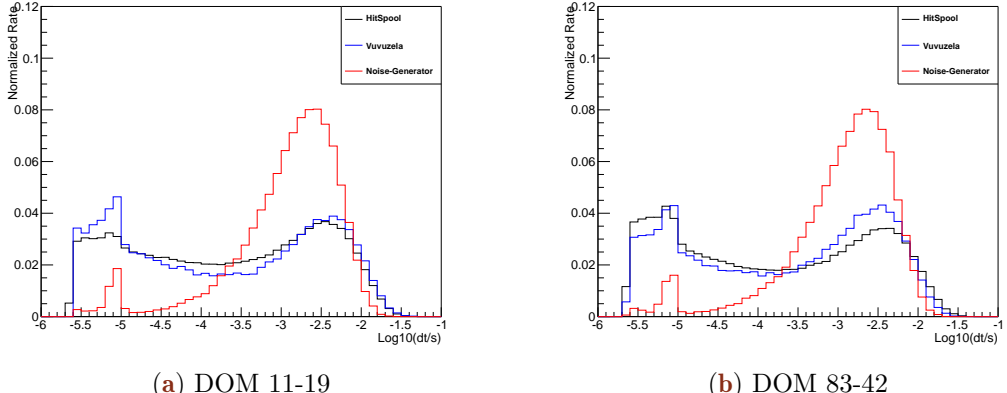


Figure 5.1 – Two examples of the original calibration work for the Vuvuzela model. The distribution of the time ("dt") between hits is shown. In black, untriggered detector data is shown. In red, a purely Poissonian noise model is shown. An afterpulsing peak is visible at 10^{-5} s. The Vuvuzela model is shown in blue. The Vuvuzela model shows improved agreement with data at all timescales.

DOMs and the number of accidental triggers due to detector noise, shown in Figure 5.2, improve significantly after inclusion of the updated noise model [1].

5.2 Limitations and Disagreement with Previous Fits

While accidental triggers with the Vuvuzela model better reproduced the rates observed in data, Figure 5.2 showed disagreement between data and simulation at very low numbers of hits. This region of the parameter space is dominated by accidental noise triggers in simulation.

An evaluation of the limitations of the previous calibration was performed in 2014, uncovering a number of possible improvements. The original fits were limited due to a number of factors. For example, the fits excluded the effect of atmospheric muons in the detector under the assumption that the hit rate per DOM due to atmospheric muons (approximately 5 Hz) is significantly smaller than the noise hit rate observed in previous calibration (about 600 Hz). Potential issues may arise from this assumption, which was not tested during original calibrations, including any potential time-correlated hits associated with muons.

Furthermore, some fits resulted in potentially-incomplete minimization. Due to the nature of the fit distributions, there existed significant degeneracy in the parameter space, leading to further difficulties.

During the fitting process, the strength of the afterpulsing peak at 9 microseconds was discovered to differ between DOMs. This effect was unsimulated, leading to convergence problems when fitting this region. In response, fits were artificially limited to timescales longer than 10 microseconds, allowing the minimizer to only observe part of the correlated noise distribution.

Because the noise hits are unlikely to satisfy the HLC conditions, timescales smaller than 6.4 microseconds were unavailable for investigation. No checks were performed for the Vuvuzela model below this limit.. The noise model itself was used down to 2 microseconds, however, resulting in uncertainty due to the extrapolation of the noise model to shorter times. The limit of 2 microseconds was implemented due to the inherent

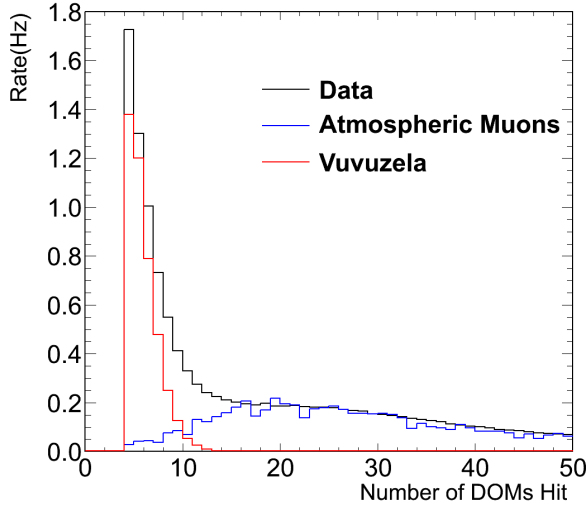


Figure 5.2 – The rates of events in DeepCore as a function of the number of hit DOMs in a cleaned hit series. The data, shown in black, consists of two components: the accidental triggers (red) and the atmospheric muons (blue). Accidental triggers produced using the Vuvuzela noise model reproduce most of the rate of events below 10 hit DOMs, although a rate disagreement remains. Image from [1].

difficulty in characterizing effects at these timescales due to artificial deadtime related to the HLC launch readout.

5.3 Low-dt Noise from Vuvuzela

In an attempt to address the imposed simulation limit at 2 microseconds, a new version of the Vuvuzela code, was created with this cutoff removed. The resulting noise, labeled *low-dt* noise for the short timescales (Δt), was used to produce a simulation of accidental noise triggers and CORSIKA muons for testing without further calibration.

The first tests, shown in Figure 5.3, used the number of hit DOMs in DeepCore events to evaluate the effect of the low-dt noise extension. The number of accidental triggers, dominant for events with fewer than 5 HLC hits, increased with the additional noise hits. The number of muons, which make up the majority of events with more than 10 HLC hits, decreased due to the use of the DeepCoreFilter, a veto described in further detail in Section ???. Both effects led to improved agreement between data and simulation.

Because the extended noise model adds hits occurring at timescales down to nanoseconds, multiple hits can occur within one waveform, leading to increased observed charge. When the noise distribution is extended below 2 microseconds, the tail of the distribution falls into the ATWD window of 322 nanoseconds, increasing the charge of noise hits in HLC DOMs. Furthermore, some fraction of the hits in a burst of correlated noise occur within the three bins recorded from the FADC for SLC hits. The result is that SLC hits due to noise no longer occur as single-photoelectron pulses, as is the case when noise hits are rare at the 10 nanosecond timescales, but as an integration of multiple single pulses. Such an effect would be most visible in the charge distribution of SLC DOMs, which are more likely to be due to noise hits than HLC DOMs.

The total charge of DOMs associated with HLC and SLC hits was evaluated to look for this effect due to the extended noise model. The result is shown in Figure 5.4. The change in the charge is observed clearly in the SLC charge distribution, where a systematic

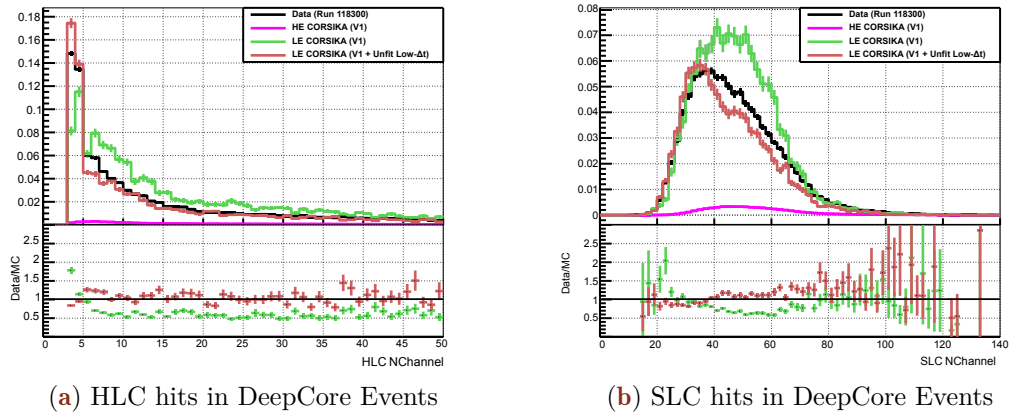


Figure 5.3 – The number of hit DOMs satisfying the (a) HLC and (b) SLC criteria described in Section 3.1.2. The distribution from 8 hours of data (black) is shown compared to a sample of CORSIKA muons at low-energy ($600 \text{ GeV} \leq E_{\text{primary}} \leq 100 \text{ TeV}$) and high energy ($100 \text{ TeV} \leq E_{\text{primary}} \leq 100 \text{ EeV}$). The addition of the low-dt extension to Vuvuzela improves the agreement between data and simulation in both HLC and SLC distributions.

shift is visible due to the low-dt extension. Both the original Vuvuzela model and the extended Vuvuzela model show significant disagreement with data in the SLC charge distribution. This demonstrated that the noise distribution at very short timescales was an important effect that deserved further attention.

The observed effect of the low-dt extension on the SLC charge distribution indicates that the distribution is sensitive to the region below 2 microseconds. The charge distribution of each DOM may therefore be used in the fitting procedure in order to characterize the low-dt end of the noise timing distribution. The effect, demonstrated in Figure 5.5, allows the investigation of a part of the distribution unavailable in previous fits.

5.4 Updating the Fitting Code

The effect of the low-dt extension on the charge distributions indicated the potential for improvement in the noise model distribution. New calibration fits for the updated noise model, referred to as *Vuvuzela V2* fits, were planned to include this extension for all DOMs.

With the opportunity to refit, a number of additional improvements were implemented. The afterpulsing peak at 9 microseconds was explicitly included in the fitting code. To account for the variability in the strength of the peak, a scale factor for the afterpulsing was included in the Vuvuzela V2 fits.

In order to include the effect of atmospheric muons, a set of Polygonato CORSIKA. The Polygonato model was selected due to the natural weighting scheme of the output files, allowing continuous simulation of the detector. Simulated files were divided into 10 microsecond long events (*long-frame* events), each containing multiple muons. The simulation was halted after photon propagation, giving a collection of muons without detector noise and effects applied.

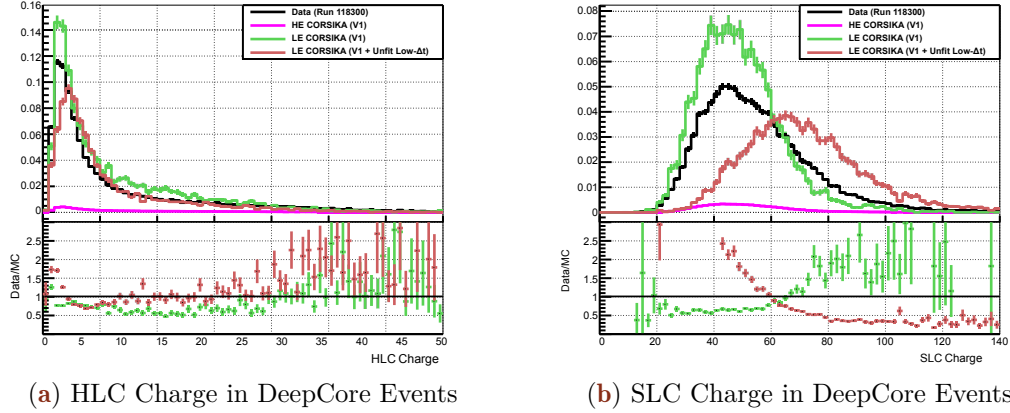


Figure 5.4 – The total amount of charge on DOMs satisfying the (a) HLC and (b) SLC criteria described in Section 3.1.2. The distribution from 8 hours of data (black) is shown compared to a sample of CORSIKA muons at low-energy ($600 \text{ GeV} \leq E_{\text{primary}} \leq 100 \text{ TeV}$) and high energy ($100 \text{ TeV} \leq E_{\text{primary}} \leq 100 \text{ EeV}$). Unlike in Figure 5.3, the charge distributions using the low-dt extension to Vuvuzela shows large disagreements with data. This is most visible in the SLC charge distribution.

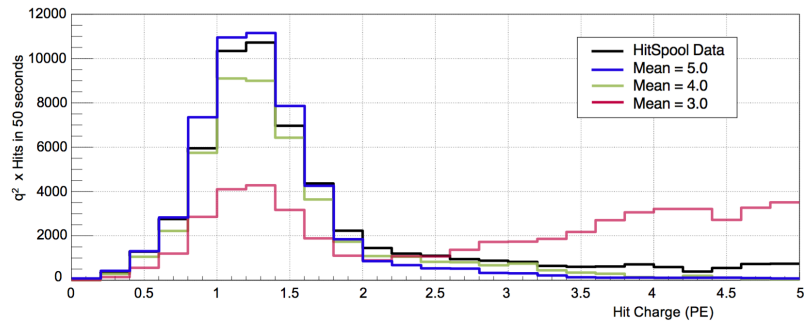


Figure 5.5 – The effect of changing the noise distribution parameters on the charge. Note the scale of the y-axis, which is scaled in order to emphasize the effect. Here, the gaussian mean is shifted from "5" (100 microseconds) to "3" (1 microsecond). All other parameters are held constant. By moving the correlated noise distribution to shorter timescales, more of distribution falls into one FADC bin, increasing the charge output for each launch.

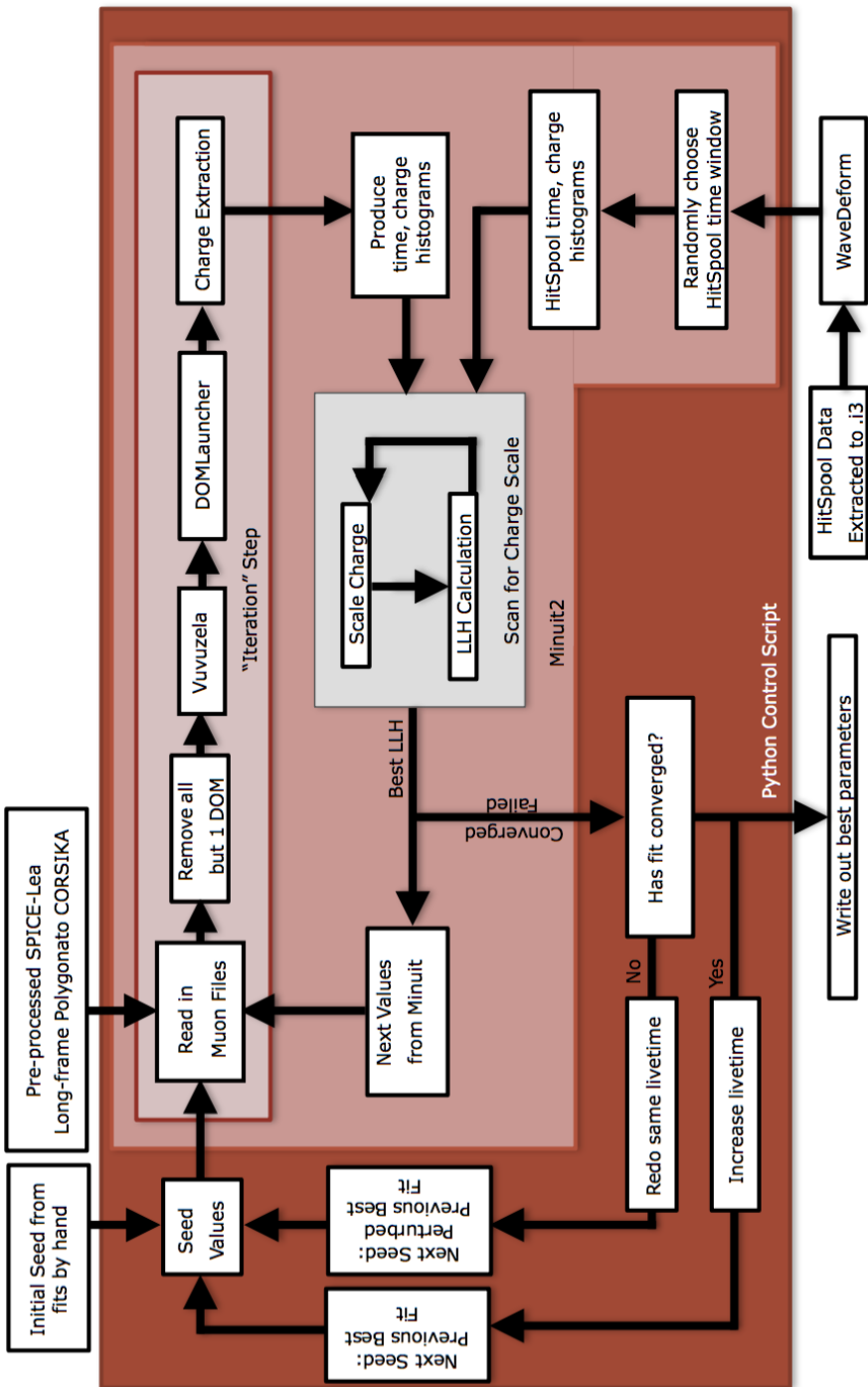


Figure 5.6 – A schematic diagram of the process used in the Vuvuzela V2 calibration fit.

The fitting process, described schematically in Figure 5.6, is divided into several parts. The code started with untriggered detector data as well as the produced long-frame CORSIKA events. The fit included a total of six explicit parameters: the five parameters from the original Vuvuzela model as well as a scale factor for the afterpulsing. Later investigations led to the introduction of a charge scale parameter to account for systematic differences between the data and simulated charge. Seeds for each parameter were taken from the Vuvuzela V1 calibration fits from 2012. Fits were performed for each DOM in parallel.

For each iteration, the long-frame CORSIKA files were filtered to remove information on all DOMs not currently being fit. The noise and detector simulation were applied using the current parameter set for the iteration. Charge extraction from the waveforms was performed using standard IceCube tools. After the simulation for a given set of parameters, histograms were produced for untriggered data and simulated hits. As in the previous fits, the time between subsequent hits is used as the primary observable of the noise behavior. In addition, the observed charge on the DOM is used as a second observable.

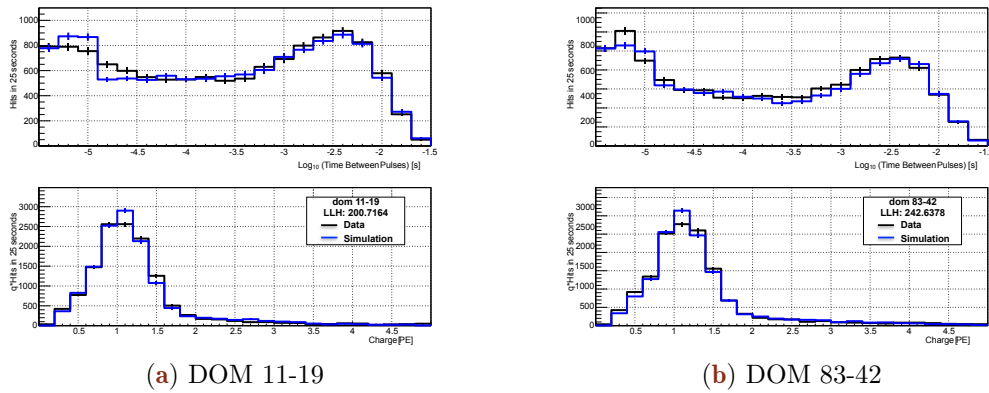


Figure 5.7 – Two examples of the new calibration fits for the Vuvuzela V2 model. The distribution of the time ("dt") between hits is shown on top. The distribution of charge is shown on the bottom. Note the y-axis of the charge distribution. In black, untriggered detector data is shown. The Vuvuzela V2 model is shown in blue. The new fits shown good agreement in both time and charge distributions.

The range of the histograms, from 6 microseconds until 1 second in the time and 0-5 photoelectrons in charge, provides sensitivity to the full range of the noise distribution. The distributions for DOMs 11-19 and 83-42 are shown in Figure 5.7.

Using the two distributions, a Poisson binned likelihood is formed. With the simulation in bin i of histogram j denoted by f_{ji} and the data hits in the same bin denoted by d_{ji} and ignoring normalization constants, the log-likelihood takes the form

$$LLH = \sum_j \sum_i^{nbins_j} d_{ji} \log(f_{ji}) + f_{ji} \quad (5.2)$$

The negative log-likelihood, $-LLH$ is minimized as a function of the fit parameters using iMinuit, a python wrapper for the minuit2 package [3, 4].

High charges from noise hits were rarely produced, limiting the effectiveness of the fitting strategy. To provide more weight to high charges, the histogram of the charges was

weighted by the value of the observed charge. This reduces the weight of very low charge launches, but increases the weight of higher charges.

Additional work showed that the charge distributions between data and simulation demonstrated disagreement in the charge distributions. This disagreement, due to miscalibration of the SPE peak in data, was accounted for by introducing a scale factor applied to the charge in simulation as a free parameter in the fit. The charge scaling applied to the simulated hits after detector simulation. To limit the computational complexity of the added parameter, the minimization over this charge scale factor is performed independently without resimulation. The form of this charge scale parameter assumes that the difference is a calibration issue in the data rather than a simulation problem. This has been shown to be the case, with an updated charge calibration now applied to data at final level.

The previous calibration attempts explicitly avoided fitting the behavior below 10 microseconds. In particular, it was noted that mismodeled afterpulsing behavior could lead to biased results in the noise parameters. The default value in simulation, assumed to be 5.93% for all PMTs, failed to take into account variations in the effects on each individual DOM. In the updated fit, the afterpulsing behavior has been investigated for each PMT by including an overall scale factor on the afterpulsing probability.

Late pulses, produced by electrons which backscatter to previous dynodes during the multiplication process, were also investigated for their effect on the goodness-of-fit in the noise distributions. These pulses occur at timescales of 50-200 nanoseconds and therefore are outside of both the SLC charge and timing distribution window. The late pulsing behavior was found to have a negligible impact due to both the rarity of late pulses as well as the lack of detailed information to constrain the distribution.

The effect of the afterpulsing parameter allowed some fits to fall into a poor local minimum. The degeneracy between parameters led to a local mimima from which the minimizer could not escape. In these cases, the probability of observing an afterpulse following a photoelectron would be moved from 5.6% to the unrealistically high value of 20%. This forced the gaussian mean of the Vuvuzela V2 model to move toward higher values and the gaussian sigma value to become unrealistically large. These fits were discovered by eye when looking at the best fit value of the afterpulsing probability, with a distinct population appearing due to this behavior. In order to constrain the fit to more realistic values, bounds were added to both the log-normal mean and afterpulsing probability for DOMs where fits showed abnormal behavior. DOMs with particularly strong afterpulsing peaks visible by eye in data were discovered. These DOMs were allowed to fit beyond the new boundary.

Due to the computational power required to produce large amounts of effective livetime at each iteration of the fitting process, a tiered approach was employed. Initial fits were seeded with the previous noise parameter fit values obtained in 2012. For these events, a coarse choice of binning both the timing and charge distributions and short effective livetime of just one minute were used. In addition, a weak tolerance value was used, allowing the minimizer to converge quickly to a reasonable minimum.

When the first tier completes the minimization process, the fit is restarted with a larger effective livetime, more bins, and a stronger tolerance using the best-fit parameters. The second tier used a 5 minute effective livetime, increasing the simulation time per iteration by a factor of 5.

The third and final tier increased the effective livetime to 10 minutes and again increased the number of bins. The final tier of minimization was the most computationally intensive and required between three and four weeks per DOM.

The fitting process for each tier continued until the minimization either converged or failed. Failure could occur due to electronics issues, such as computing cluster downtime, or due to a limit of 10000 iterations set in the minimizer to prevent issues with maximum processing time available on the computing cluster. In the case of a failure, the fitting tier was restarted with a new set of seed values. The new seed values were selected from a gaussian distribution centered on the previous seed with a width of 5%. The fit was then restarted. This process was continued until the third tier was complete for all DOMs.

5.5 Results of New Noise Fits

New calibration fits were completed over the course of two months for nearly all DOMs in the IceCube detector. String 25 and DOMs previously disabled due to malfunction are absent from the untriggered data, taken in 2014, used here and were therefore left unfit. The parameters for string 25 were selected using the average of all other fits.

The Vuvuzela V2 fits were checked after convergence in Figure 5.8 and Figure. One notable feature is the number of DOMs with afterpulsing at and beyond the fitter boundary. The likelihood values associated with these fits, however, appear to be consistent with other fits. Due to a planned overhaul of the afterpulsing simulation, the fit values of the afterpulsing probabilities have not been adopted for simulation. Therefore, no further investigation of the probabilities has been pursued.

The thermal rate is associated with the electronic noise, which should show increasing rate with increasing depth due to the rising temperature. This effect is only weakly apparent in Figure 5.9.

Other parameters should be independent of depth. As a test of the fits, each of the other parameters is plotted as a function of depth as well. No significant correlation is observed.

Finally, the likelihood values should be independent of depth. This final test, shown in Figure 5.10, shows surprising results in at least two ways: a 'band' structure appears in the plot. and there appears to be a depth-dependent decrease in the likelihood value, indicating that the lower part of the detector yields better fit results. This was initially unexpected, given that the noise is an internal property of the DOM and not of the surrounding medium.

This effect occurs due to a combination of factors. It is worth noting that the noise measurements of each DOM are not fully independent. The fits themselves use the long-frame CORSIKA to model the effects of muons in the untriggered data from the detector.

This leads to two subtle limitations in the fitting process. The long-frame CORSIKA is produced with a single flux model, in this case the Polygonato model used in CORSIKA [5]. Because the long-frame CORSIKA cannot be reweighted to other models, uncertainties or mismodeling in the muon flux can lead to disagreement in the fitting of noise parameters. The muon flux decreases with increasing depth, resulting in a lower muon contamination, and consequently smaller effects from mismodeling of the muon background, for deeper DOMs.

In addition, the long-frame CORSIKA implicitly assumes a single model of the ice for photon propagation. Mismodeling of the scattering and absorption of the ice therefore may also give rise to disagreement in the noise calibration. While large-scale properties of the ice are believed to be well-reproduced by the chosen ice model, SpiceLea [6], there will inevitably be remaining disagreements.

The net effect of these two assumptions in the muon simulation is effectively correlated with the convolution of the ice model and the muon flux. In particular, the best fits

occur where the DOM is either A) well-shielded from light due to muons by the large overburden or B) well-shielded due to large absorption in the ice. In both cases, the contamination from light due to muons in the fitted time and charge distributions will be small, leading to a more ‘pure’ noise distribution that is well-fit by the Vuvuzela V2 noise model.

The sensitivity of the noise calibration procedure to underlying assumptions of both the muon flux and the absorption properties in the detector imply that little further improvement is likely without additional work on one or both issues. Simulation of long-frame CORSIKA is, unfortunately, not possible with newer flux models at this time. As the primary uncertainty affecting the goodness-of-fit appears to be due to the visibility and flux of the muons themselves, merely updating to a newer model of the ice will be unlikely to significantly improve the current fit parameters.

The newly calibrated low-dt Vuvuzela was provided to the IceCube simulation group in January of 2015 and quickly integrated into the low-energy simulation chain. New neutrino, muon, and accidental noise trigger simulations were produced soon thereafter. The updated noise model shows significantly better agreement in both the total charge distribution and the number of hit DOMs for both HLC and SLC+HLC hits. The rate of accidental triggers improved relative to previous calibrations, with the remaining rate disagreement reduced from 50% to approximately 15%. Negligible effect was observed in the low-energy neutrino events at final level for existing samples.

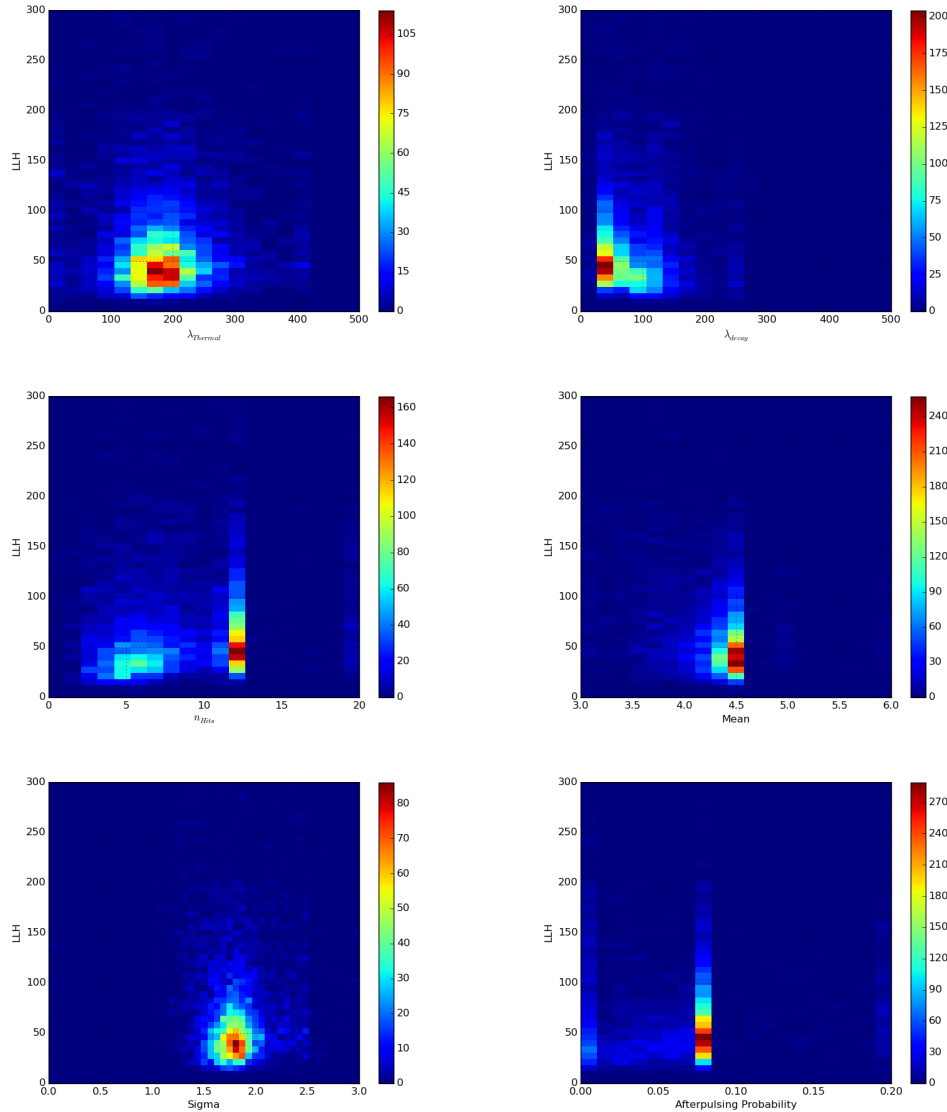


Figure 5.8 – The distributions of each new fit parameter in the Vuvuzela V2 model. The colorbar scale shows the number of DOMs in each bin. The effects of fit bounds are visible in most distributions except for the thermal noise rate and the width of the log-normal distribution describing the non-Poissonian noise.

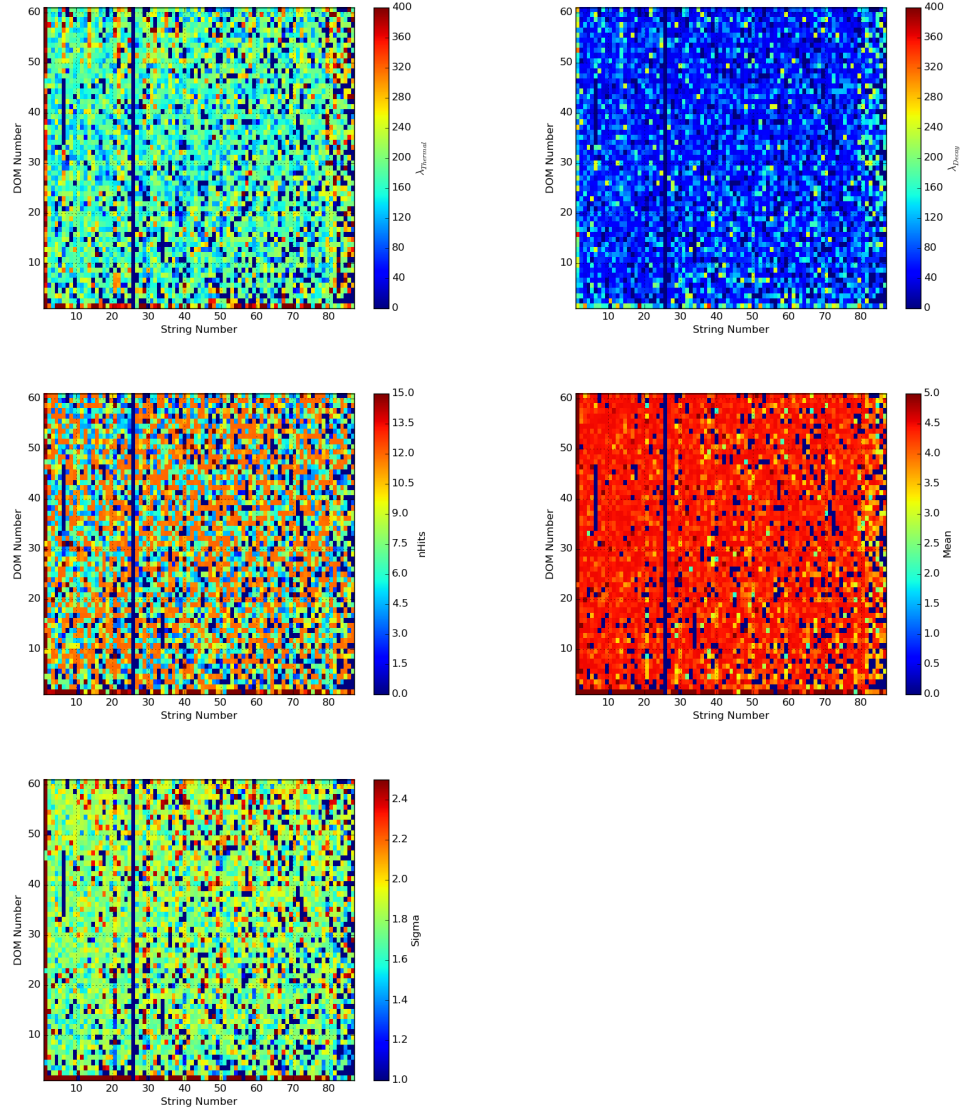


Figure 5.9 – The distributions of each new fit parameter in the Vuvuzela V2 model as a function of the string and DOM number. Note that the top of the detector is at the bottom of this plot. No parameter appears to be correlated with depth. DOMs on string 25 are missing from the dataset. In addition, DOMs which are disabled due to malfunction are also unavailable.

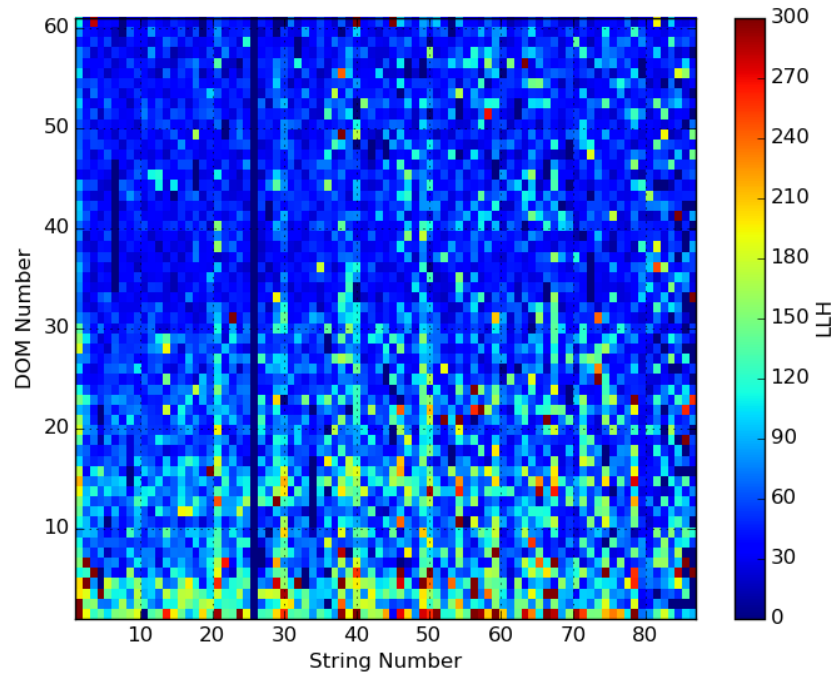


Figure 5.10 – The log-likelihood as a function of string and DOM number for the Vuvuzela V2 fits. Note that DOM 1 is at the top of the detector and DOM 60 at the bottom. The likelihood value was expected to be independent of depth, but shows some structure. These structures are correlated with both the ice model and the muon flux.

Low-Energy Muon Simulation

The updates of the noise simulation provide one reduction of background uncertainties in the appearance analysis. Another large uncertainty existing in the analysis is due to the limited simulation statistics of the atmospheric muon samples.

For low-energy oscillation analyses, the simulation of muons has proven difficult due to the computationally intensive simulation scheme. Large numbers of simulated events are produced for general IceCube analysis use, although the vast majority do not reach DeepCore. In response, previous analyses [7, 8, 9, 10] have developed methods to reuse data events which fail the selection as a model the background at final level. Severely limited simulated statistics from the CORSIKA generator precluded strong checks of these samples, but good fits were obtained with oscillation measurements consistent with other experiments.

For the search for tau neutrinos, new background generation techniques were used to more robustly model atmospheric muons. Two new generation schemes for low energy IceCube analyses are discussed here. The first, briefly discussed in Section 6.1, provided the final background sample used in the search for tau neutrinos. The second method, discussed in Section 6.2, is more experimental, but shows potential to further improve the background generation efficiency substantially for future analyses.

6.1 CORSIKA Generation In DeepCore

In IceCube, most simulation is produced centrally for use by the entire collaboration. This is especially true for background simulation produced with the CORSIKA generator. CORSIKA simulation, using the 5-component scheme discussed in Section 4.1.1, is the most common background simulation used in IceCube. These simulations are broken into two energy ranges based on the simulated primary particle energy in order to allow efficient generation of rare, high energy events. These are "low energy" CORSIKA, produced with primary energies $600\text{GeV} \leq E_{\text{prim}} < 10\text{TeV}$, and "high energy" CORSIKA, with energies $10\text{TeV} \leq E_{\text{prim}} < 100\text{EeV}$. These samples are produced in the upper atmosphere using the CORSIKA 5-component mode, then propagated to the detector, losing energy in transit.

Unlike MuonGun, CORSIKA generation does not currently possess a method to target specific sections of the detector. Instead, muons are pass through a upright cylinder of radius 800 m and length 1600 m around the center of IceCube. This allows uniform coverage useful for a wide range of analyses.

The centralized CORSIKA simulation in IceCube results in high statistics datasets used by all analyses in the collaboration. The production of these sets is computationally intensive, requiring hundreds of CPU-years and GPU-years worth of processing time in order to reach sufficient statistics. The number of unweighted simulation events and required computational resources required for centralized CORSIKA sets is shown in Table 6.1. Included is the 'simulation efficiency', the average number of events produced per computational year.

$$\epsilon = \frac{N_{\text{final}}}{t_{\text{CPU}} + t_{\text{GPU}}} \quad (6.1)$$

Generator	Sim. Req.	Number of Events			ϵ
	CPU	GPU	Generation	Final Level	
CORSIKA	188.9 Years	48.75 Years	8×10^{12}	284	1.20

Table 6.1 – The simulation requirements needed for the production of the standard CORSIKA sets in IceCube. The number of events reaching final level of the appearance search (Section 7.6.3) are shown. CORSIKA simulations are computationally intensive, but inadequate for low energy analyses in IceCube.

For analyses using DeepCore, the CORSIKA generation scheme results in many muons that are easily rejected. Events which interact solely outside of the DeepCore fiducial volume are removed early by a veto algorithm discussed in Section ??, reducing the background statistics from $O(10^{12})$ to $O(10^6)$. Additional cuts reduce this number further, with the GRECO selection described in Chapter 6.3 removing all but 284 events from an initial sample of 8×10^{12} . These events represent nearly 10% of the final level sample after weighting.

The final sample of muons in GRECO is too statistically limited to be of use in oscillation analyses. While previous analyses have used data-driven estimates of the background shape, verification of such techniques is itself limited by the simulated background statistics as well. In order to produce sufficient statistics for use in the appearance analysis, new background simulation techniques were necessary.

6.2 MuonGun for DeepCore

As described in Section 4.1.1, the MuonGun generation scheme provides a method to target specific parts of the detector. Doing so allows for *biased generation*, leaving some regions undersimulated while increasing the simulation statistics in the target volume. The limited size of the DeepCore fiducial volume provides an ideal use case for this biased generation.

In MuonGun, the muons are produced on a *generation cylinder* with a radius of 800 meters and length of 1600 meters, matching the final muon positions of the CORSIKA generator. The muons are pulled from a power law spectrum of the user's choice. An offset power law distribution is selected for this work in order to align with previous analyses [11].

$$f(E) = (E + E_0)^\gamma \quad (6.2)$$

where E is the energy of the muon at the generation cylinder, E_0 is an offset energy for generation, and γ is a configured spectral index. For this thesis, a power law is selected with a soft spectral index of -5, an offset of 700 GeV, parameters which correspond to the defaults assigned for example code. Note that the cosmic ray spectral index is approximately -2.7. The steep spectral index selected for generation leads to overgeneration of very low energy events. These events are expected to produce little light in the outer detector, making them difficult to identify from vetoing algorithms. Low energy muons are therefore expected to dominate the low energy background at final level of the GRECO sample.

CORSIKA events observed in the GRECO analysis at Level 5 (Section 7.4.3), the last cut level with significant CORSIKA statistics available, are used to select an energy range for MuonGun simulation. These events are shown in Figure ?? The lower energy limit, 160

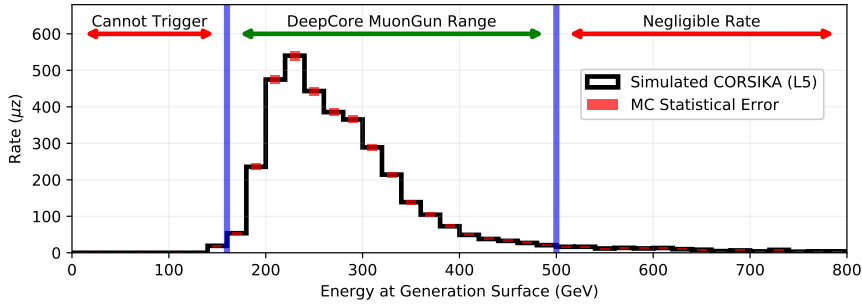


Figure 6.1 – The distribution of CORSIKA muon energies at the MuonGun generation surface using GRECO Level 5 muon events. Very few events trigger are seen below 160 GeV and less than 5% of events occur beyond 500 GeV. These two energies set the bounds for the MuonGun generation. MuonGun simulation has also been produced and tested above 500 GeV, but no simulated events survived to final level in GRECO.

Generator	Sim. Req.		Number of Events		ϵ
	CPU	GPU	Generation	Final Level	
CORSIKA	188.9 Years	48.75 Years	8×10^{12}	284	1.20
MuonGun	10.27 Years	12.11 Years	3×10^9	2486	111.08

Table 6.2 – The simulation requirements needed for the production of MuonGun simulation for DeepCore. The MuonGun simulation is nearly two orders of magnitude more efficient at producing statistics at final level in the appearance analysis.

GeV, is selected by using CORSIKA simulation to identify the minimum energy required for a muon at this surface to reach and trigger the DeepCore detector. A high energy limit on the MuonGun generation was set at 500 GeV, beyond which less than 5% of events remain. The energy range selected, shown in Figure 6.1, includes more than 95% of the distribution of CORSIKA events.

The angular spectrum of the MuonGun simulation is created by setting a *target cylinder* toward which the generated muon must intersect. For this work, the DeepCore fiducial volume is used as a target, encompassing a cylinder with radius 150 meters and length 500 meters centered on the geometric center of DeepCore at $x=(46.3, -34.9, -300)$.

A sample of muons was created using these settings of MuonGun and the resulting resource requirements are shown in Figure 6.2. The efficiency improvement from changing to MuonGun is substantial, increasing from 1.20 CORSIKA events/year to 111.08 MuonGun events/year, an increase of nearly two orders of magnitude. The MuonGun generation for DeepCore proved to be a far more efficient method of generation of low energy background events than the centralized CORSIKA simulation produced for the collaboration.

This simulation scheme has limitations. Because the target volume is small, events which do not enter DeepCore are not included in these sets. These events form a substantial background at early selection levels and cannot be ignored. For this reason, CORSIKA muons are required for the development of selections and will be used in the Chapter 6.3 until Level 5 (Section ??).

The generated statistics are useful for analyses at or near final level, where muons outside of DeepCore are no longer a dominant source of background. The newly produced MuonGun statistics are used to model the muon background after Level 6 (Section ??).

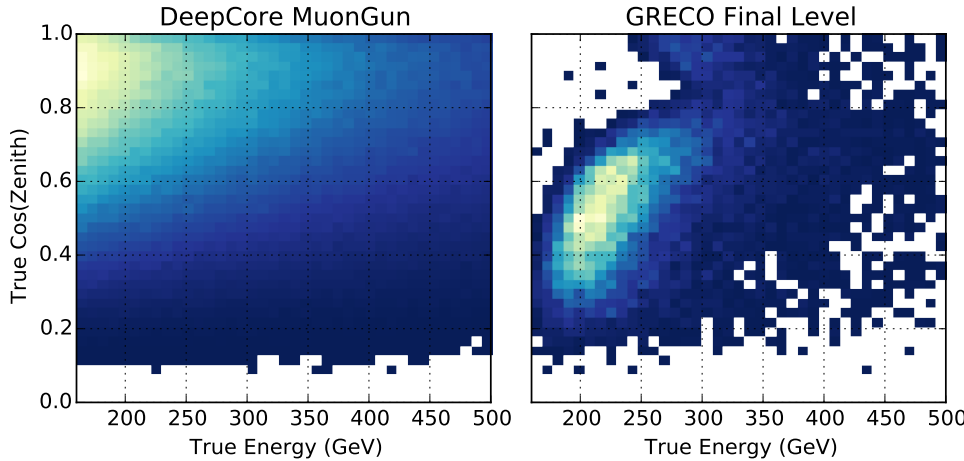


Figure 6.2 – The generated spectrum from MuonGun in energy and zenith angle compared to the events reaching the final level of the GRECO event selection. Both distributions have been normalized to 1. The majority of events produced by MuonGun are downgoing and low energy. These events do not reach final level.

6.3 Simulation Efficiency with KDE Prescales

After processing to the final level of the GRECO event selection (see Chapter 6.3), the background MuonGun simulation retains 2486 simulated events of the original sample of 3×10^9 generated events. The sample is sufficient for the search for appearance, but further improvements are possible.

While the previous section focused on improvements based on the simulation volume using MuonGun, inefficiencies still exist in the energy and zenith angle spectrum of the generated events. This inefficiency is shown in Figure 6.3. The majority of the events produced by MuonGun are very downgoing ($\cos(\text{zenith}) \approx 1$) and low energy. These events are noticeably absent from the final level sample.

In addition to the energy- and zenith-dependent effects, the GRECO selection exhibits strong azimuthal selection bias. This arises due to three effects. The first is the offset between the center of IceCube (and therefore the center of the generation volume) at $(x, y) = (0, 0)$ and DeepCore at $(x, y) = (46.3, -34.9)$. Due to this offset, the distance required to reach the DeepCore fiducial volume at an azimuthal angle around 150 degrees is longer than the corresponding distance at 0 degrees. This gives rise to an azimuthal effect appearing as a sinusoidal variation of the minimum generated energy of events at final level.

The second is the regular hexagonal structure of the IceCube volume, with long "corridors" through which muons may reach DeepCore without crossing any strings. Cuts designed to look for hits left in the veto region produce these azimuthal biases when muons close to strings are more likely to be identified and removed than those further from strings (see Section ??).

Finally, the DeepCore detector is not fully surrounded by an even layer of strings. This may be seen in Figure 3.8, where a layer of four strings is available for muon identification in the top left, but a layer of only three strings is available on the bottom right. Events entering the detector from this direction are more likely to reach DeepCore without being tagged, resulting in a larger acceptance of events around 300 degrees.

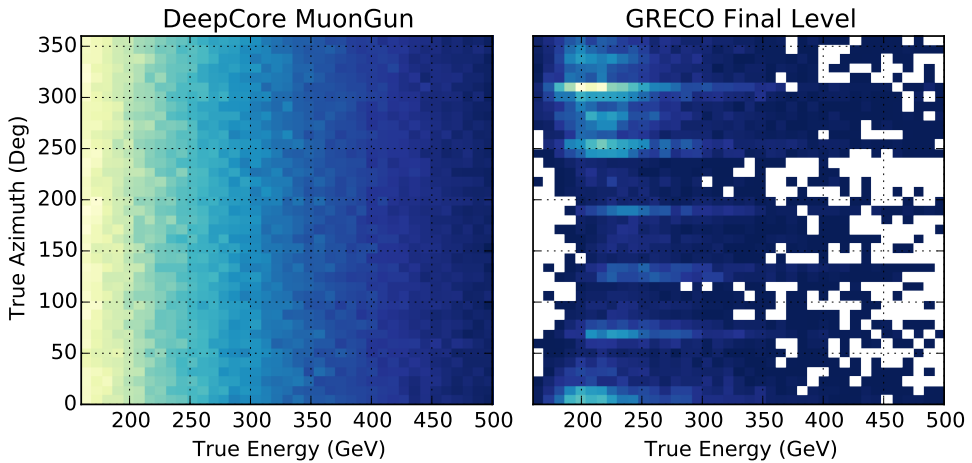


Figure 6.3 – The generated spectrum from MuonGun in energy and azimuthal angle compared to the events reaching the final level of the GRECO event selection. Both distributions have been normalized to 1. Events in the final level sample are strongly biased in azimuth due to the geometry of the detector.

In order to improve simulation statistics at final level, the existing MuonGun simulation scheme was modified to include an energy-, zenith-, and azimuthally-dependent prescale factor. This approach, here referred to as a *KDE prescale*, allows simulation to be produced with a known bias matching that of a given set of input files.

In this scheme, the *kernal density estimator (KDE)* from SciPy [12] is applied to all remaining events at final level of the GRECO event selection. The KDE uses a Gaussian kernal to represent each event in energy, zenith, and azimuth. The resulting KDE is normalized to produce an approximation of the final selection probability density function. In the new simulation scheme, an event is produced using standard settings for MuonGun generation described in the previous section. Immediately following generation, the probability of the new event reaching final level is calculated from the KDE, with typical values of approximately 10^{-4} for a likely event and 10^{-9} or lower for unlikely events. A prescale multiplicative factor of 10^5 is used to set the overall probability scale. The product, p of the prescale factor and KDE probability is used in order to accept or reject events. The value is interpreted as an acceptance probability and may not exceed 100%. Any values for which this may be the case are directly set to 100%.

Using a random number generator, this p factor is used to retain or reject the muon event. The simulation then proceeds as normal, with photon propagation, detector simulation, triggering, and filtering.

When events need to be weighted by a flux model, the p factor must be included as well. The weighting scheme utilizes the standard MuonGun weighting code to find the event weight. The total weight is then scaled by $\frac{1}{p}$ to correct the rates and uncertainties for the simulated events.

The results of this experimental method are shown in Table 6.3. By removing unlikely events early in the simulation chain, the required computational resources are further reduced compared to the general CORSIKA simulation sets used by the IceCube collaboration. While the number of events at final level is comparable to the MuonGun methods described in Section 6.1, the required time for simulation is reduced to less than 1 computation-year.

Generator	Sim. Req.		Number of Events			ϵ
	CPU	GPU	Generation	Final	Level	
CORSIKA	188.9 Years	48.75 Years	8×10^{12}	284		1.20
MuonGun	10.27 Years	12.11 Years	3×10^9	2486		111.08
MuonGun+KDE	75 Days	175 Days	9×10^8	3588		5241.92

Table 6.3 – The simulation requirements and number of events for each muon generation scheme. The use of the KDE prescale improves the simulation efficiency by a factor of 50x compared to the DeepCore MuonGun simulation method described in Section 6.1.

Further optimizations are possible at the expense of accuracy. For example, the oversizing methods described in Section 4.2.2 may be used to reduce the number of propagated photons. Using $N_{OS}=3$, the GPU simulation requirements are reduced by approximately 8x, leading to a total simulation efficiency of 13527.55. The oversizing is known to cause a small bias in the simulated photon arrival time, potentially leading to bias in particle reconstructions. Oversizing should be used with care in order to minimize or eliminate these biases.

The KDE prescale demonstrated here used only unweighted events due to limitations in the SciPy software. The KDE therefore encodes some bias towards the production of low energy muons due to the soft spectral index of the MuonGun DeepCore generation. Other implementations of multidimensional KDEs can accept event weights [13, 14]. The use of these algorithms would be beneficial and remove some dependence on the generation characteristics of the source events used for building the KDE.

The simulation using KDE prescales is limited by the events used to form the KDE. If too few events are used, the KDE may not adequately represent the shape of the underlying spectrum, leading to little gain in efficiency. Likewise, if a region is underrepresented in the sample, the KDE may not describe the distribution of events in this region. Care should be taken in order to check for unsimulated regions before using the KDE prescale to avoid these situations.

The use of the KDE prescale method shows substantial promise in improving simulation efficiency. Work is ongoing within the IceCube collaboration at the time of this writing to investigate use of the method for DeepCore analyses. If adopted, the improved simulation efficiency may allow future analyzers to significantly reduce the statistical uncertainty in the simulated background samples.

GRECO: An Event Selection at the Limits of DeepCore

The search for appearance in atmospheric neutrinos requires a selection of neutrino candidate events. The events passing the SMT3 trigger in DeepCore, however, are dominated by Muons, at 280 Hz [15] compared to a neutrino rate of about 4 mHz.

In order to remove the atmospheric muons, an *event selection* is necessary. The GeV Reconstructed Events with Containment for Oscillations (*GRECO*) event selection is presented here. This selection was developed for the appearance analysis and reduces the atmospheric muon rate to around 0.07 mHz while retaining around 0.7 mHz of atmospheric neutrino events.

The selection consists of multiple stages, or *cut levels*. Each will be presented sequentially.

7.1 Hit Cleaning

Following the triggering of the detector, the waveforms of each hit must be extracted to obtain information about the charge of events. Not all recorded pulses are the result of muon or neutrino interactions in the detector, however. To identify hits relevant for the study of muons or neutrinos, a number of *hit cleaning* algorithms are used.

7.1.1 Pulse Extraction

The extraction of charge and timing information from recorded waveforms is performed using the *wavedeform* module, which accepts and processes the information from the launches in each triggered event. Wavedeform attempts to reconstruct the original charge information from the digitized waveform information.

Wavedeform uses a parametrized version of the PMT pulse associated with a single photoelectron shown in Figure 4.3 extended to include a timing dimension describing the timing profile of the PMT amplification process. Beginning with a single pulse template, a least squares minimization is performed to find the best-fit time of a single pulse in the observed waveform. Additional copies of the pulse template are added and new minimizations are performed until the goodness-of-fit improvement from additional pulses is negligible. The resulting sets of pulses, including associated timing and normalization, are returned as *reconstructed pulses*, more commonly referred to as simply *pulses*. These pulses represent the best-fit recreation of the analog pulses in the PMT prior to the digitization process.

Both HLC and SLC waveforms are fit, although the limited information in SLC waveforms necessarily results in the loss of information. When available, information from the ATWD is provided a larger weight relative to the information from the FADC due to the finer binning in time, allowing for more detailed information on PMT behavior near the beginning of the launch of the DOM.

7.1.2 Hit Cleaning

In general, a set of pulses from a given event, referred to as a *pulse series*, contains a significant number of pulses due to random detector noise. These additional pulses are not useful for understanding the particle interactions and are therefore typically removed during processing. There exist multiple ways to identify pulses likely to be due to detector noise, three of which will be detailed in order from most strict to most accepting.

The most strict cleaning results from the exclusive use of local coincidence information. This type of cleaning is referred to as *HLC cleaning* and is shown in Figure 7.1. By selecting only pulses that result from DOMs satisfying the HLC criteria discussed in Section 3.1.2, the resulting pulse series can be cleaned of nearly all detector noise. No additional processing is necessary, although cleaning the pulse series based solely on local coincidence criteria comes at the expense of a potentially significant amount of information about the event, since all SLC hits are removed.

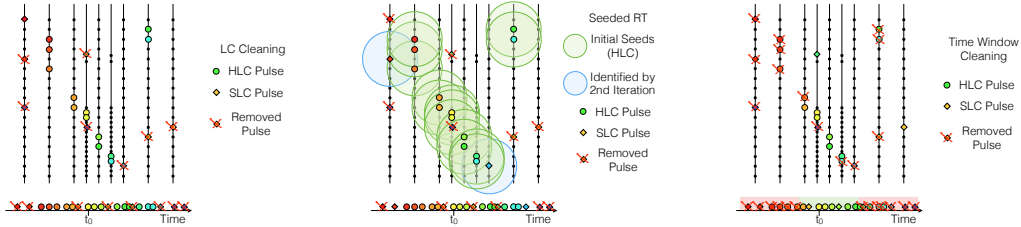


Figure 7.1 – An illustration of the LC, SeededRT, and time window cleaning methods. (Left) All SLC pulses are removed while all HLC pulses are retained. (Middle) Pulses are removed based on time and distance from nearby HLC DOMs, allowing some SLC pulses to be accepted. (Right) Pulses are removed using the time relative to either the trigger (STW) or the maximum pulse density in time (DTW).

SeededRT Cleaning

Instead of simply using HLC hits, additional processing may be used to identify potentially interesting SLC pulses as well. The *SeededRT (SRT)* algorithm is one such algorithm, requiring a seed, radius, and time in order to search for additional information in the event as shown in Figure 7.1. SeededRT begins with a subset of "interesting" pulses, often a selection of the HLC pulses, as a seed. Once a seed is selected, a sphere is drawn around each seeded DOM. Any nearby DOMs within the sphere and time window are added to the output pulse series. Once all seed DOMs have been checked, a new seed is created composed of the all current output pulse series. The process is repeated until no further pulses are discovered.

The most effective set of parameters is dependent on the detector geometry, since a given radius sphere will contain more DOMs in the DeepCore fiducial than the same sphere outside of DeepCore. Because of this, different settings are chosen for these two regions. In the less dense IceCube detector, a typical value for the radius is 150 m and for the time window is 1000 ns. In DeepCore, these values are typically halved, with a radius of 75 m and a time window of 500 ns.

The SeededRT algorithm is commonly used in IceCube, allowing for a pulse series with minimal noise contributions while finding most hits due to muon or neutrino interactions.

Time Window Cleaning

The most permissive pulse cleaning algorithm results in very little loss in pulses due to particle interactions, but allows nearly all noise pulses into the final hit series. This *Static Time Window* cleaning, often referred to using just the acronym *STW* cleaning, looks for pulses near the time of the trigger. For DeepCore processing, any pulses more than 4 microseconds before or more than 6 microseconds after the SMT3 time are removed.

There exists a second type of time window cleaning applied more rarely, but used in the GRECO selection. The *Dynamic Time Window* cleaning, hereafter *DTW* cleaning, is a time window cleaning algorithm that uses the maximum pulse density in time to find the most likely interaction time of a muon or neutrino. The timing window is placed around this time instead of around the trigger. DTW cleaning is generally chosen with a significantly tighter window, often consisting of only a few hundred nanoseconds compared to the multiple microseconds used in the *STW* cleaning.

Time window cleaning is typically used in combination with additional cleaning methods, resulting in little loss in useful signal due to the wide time window (in *STW* cleaning) or in a very pure set of hits likely to be due to unscattered light.

7.2 Level 1: The DeepCoreFilter

Triggers are generally designed to be as accepting of the proposed physics signal as possible, regardless of the background rates. Typically, limitations exist solely in the processing and storage capabilities in order to prevent the unintentional loss of valuable information. After triggering, various filters may be applied with the sole purpose of removing the collected background. For the purposes of this document, the only filter considered is the *DeepCoreFilter*.

The DeepCoreFilter proceeds by splitting the pulses identified by the SeededRT cleaning into "veto" and "fiducial" pulses, with each DOM given a designation based on its position in the detector as described in Section 3.1.6 [16, 1]. The average and standard deviation in time are first calculated for the fiducial pulses. All hit DOMs with the first pulse occurring more than one standard deviation away from the mean time are removed from the fiducial pulse series in order to further limit the contributions from noise pulses.

With the updated fiducial pulse series, a center of gravity, or *CoG*, of the remaining DOMs is calculated.

$$\vec{x}_{CoG} = \frac{\sum_i^{DOMs} \vec{x}_i}{N_{hits}} \quad (7.1)$$

The "corrected" average time of the fiducial pulses is then calculated by assuming that the pulse is due to light emission at the CoG, as would be the case for a point-like interaction of a cascade event.

$$t_{CoG} = \frac{\sum_i^{DOMs} t_i^0 - \frac{\vec{x}_i - \vec{x}_{CoG}}{c_{ice}}}{N_{hits}} \quad (7.2)$$

where t_i^0 denotes the time of the first observed pulse and \vec{x} the position of each DOM. All veto pulses are then compared to this CoG time and position by calculating an effective particle speed, v .

$$v = \frac{|\vec{x}_{CoG} - \vec{x}_{hit}|}{t_{CoG} - t_{hit}} \quad (7.3)$$

Muons passing through the detector will do so at the speed of light, 0.3 m/ns. Unscattered hits left behind in the detector show this peak clearly for muons. Low energy neutrino events, on the other hand, typically begin in DeepCore, with hits outside of the fiducial region following hits inside. These neutrino events show a peak at negative speeds.

The DeepCoreFilter is the first step in a low energy analysis in IceCube and is used in many analyses [1, 17, 7, 8, 9]. The algorithm reduces the atmospheric muon background from 280 Hz to approximately 17 Hz while retaining 99.4% of neutrino events which begin in DeepCore [16].

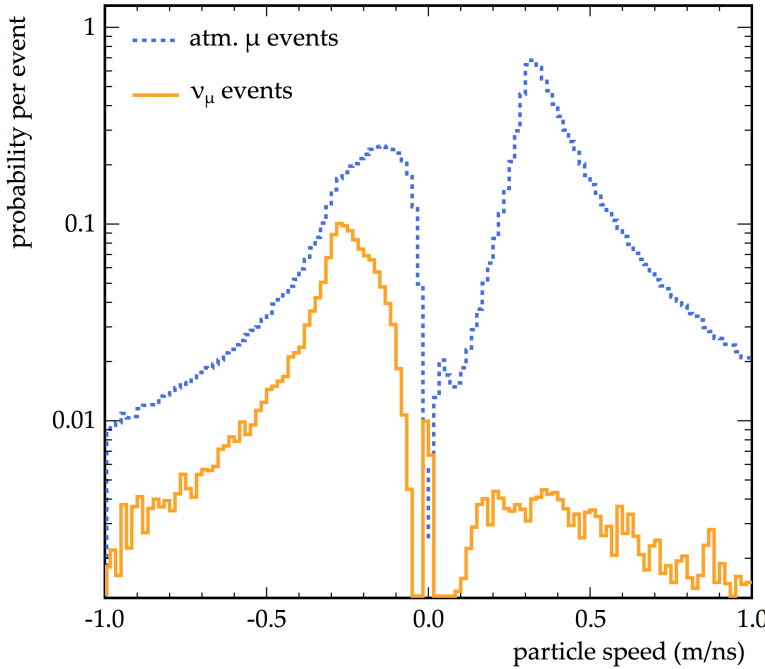


Figure 7.2 – The distribution of effective particle speeds used by the DeepCoreFilter to identify and reject muons. Because muons interact first outside of DeepCore, a large peak is visible at speeds around 0.3 m/ns, the speed of light. Figure from [16]

7.3 Low-En Level 3 Cuts

After the DeepCoreFilter is used to remove events, variations of hit cleaning algorithms and reconstructions are used. This processing stage, *Level 2*, does not remove events from the selection and will not be discussed here.

Following the Level 2 processing, the *Low energy Level 3* cuts are introduced. These cuts are standardized and used in all DeepCore oscillation analyses. The Level 3 processing stage introduces the structure of the remaining cut levels by using a set of *accidental event cuts* and *muon cuts*.

After the DeepCoreFilter, approximately half of the remaining rate consists of muons. The remainder is due to accidental triggers due to random detector noise due to the low trigger threshold used in DeepCore.

7.3.1 Accidental Rejection at L3

Three cuts are introduced at Level3 in order to reduce the observed number of accidental triggers. Events are required to have at least pulses and a total charge of at least 3 PE in a 250 ns DTW cleaned pulse series in the DeepCoreFiducial region. This removes events which have reached Level 3 processing via random detector noise in the fiducial region.

In addition, the *NoiseEngine* algorithm is used to identify accidental triggers [1]. NoiseEngine uses the relative direction between each pair of hits to search for directionality of the event. Events with fewer than three hit pairs pointing in the same direction fail the algorithm and are rejected. After the NoiseEngine algorithm, more than 96% of accidental triggers are removed from the analysis.

7.3.2 Muon Rejection at L3

The removal of muons relies on some understanding of the characteristics of these events at Level 3. Muons at this level are generally bright enough to be identified by hits in the outer part of the detector, known as the *veto region*. Because neutrino candidates of interest in this search are low energy, no light emission is expected in the veto region due to neutrinos. This may be used to identify muons using cuts described here.

First Hit Z Position

Because the muon tracks are primarily steeply inclined, most will leave hits in the upper part of the detector. Neutrinos of interest in the search for appearance will primarily emit light within the DeepCore fiducial volume, leading to little or no light emission in the top half of the detector. This difference between neutrino and muon emission in the upper part of the detector can be used to identify background muons. The position of the first hit in a STW+SRT cleaned pulse series consisting of DeepCore fiducial hits is used to look for muons using this principle. Any event with a first hit above $Z=-120$ m is removed.

NAbove200

The total charge of recorded hits occurring in the top of the detector is also used in the analysis. This variable, known as *NAbove200*, counts the amount of charge occurring before the SMT3 trigger above a depth of -200 meters. If more than 12 DOMs are hit above $Z=-200$ m, then the event is removed.

RTVeto

The SeededRT algorithm is useful for removing accidental noise hits in the detector. It may also be used to find clusters of hits due to muons in the outer part of the detector as well. This technique, known as *RTVeto*, uses the SeededRT algorithm to identify the largest cluster of pulses in the outer detector. The number of hits in this cluster is used to identify atmospheric muon events. The RTVeto algorithm uses a radius of 250 m and a time window of 1000 ns for both DeepCore and IceCube DOMs.

The cut is used in combination with the total amount of charge observed in the DeepCore fiducial region to define a few separate cut conditions. For the purposes of this search, only the lowest energy version is relevant. In this case, any event with a cluster of 4 or more hit DOMs in the outer detector is removed.

C2QR6

Atmospheric muon events at Level 3 tend to leave long tracks and take $O(3 \mu\text{s})$ to cross the detector. Oscillation neutrino events produce small light patterns small due to the low energies involved, with light being deposited quickly. The difference in the light emission profile of the two event types may also be exploited to reject atmospheric muons background events.

Type	IceCube Processing		
	Any Filter	DC Filter	Low-en L3
CORSIKA	990598	9178	969.818
MuonGun	60669	2982	442.493
Accidentals	35855	8117	283.559
ν_e	1.842	1.721	1.262
ν_μ	11.317	6.360	4.758
ν_τ	0.293	0.270	0.206
MC Total*	1026466	17303	1260
Data	1154426	19092	1092

Table 7.1 – The event rates after the Level 3 cuts in GRECO. The total simulated rate is calculated using CORSIKA events and ignoring MuonGun. The data rate is estimated from a burn sample of 10 runs at Level 3. Rates are given in mHz.

To test the deposition time for light in each event, the *charge ratio in 600 ns* (*QR6*) is calculated as the ratio of charge observed in the first 600 ns and the total amount of observed charge.

$$QR6 = \frac{\sum_i^{t_i < 600} \text{hits}}{q} \sum_i q_i \quad (7.4)$$

Here the time is measured relative to the first observed hit in a STW+SRT pulse series. Atmospheric muons will tend to deposit light over a longer timescale, resulting in a charge ratio near 0. Neutrinos will deposit light quickly, with a charge ratio near 1.

The algorithm relies sensitively on the first observed hit. The observation of noise hits before the particle interaction can lead to an erroneous definition of the time window. In order to reduce this possibility, the first two hits may be ignored for the calculation. This form, the *cleaned charge ratio in 600 ns* (*C2QR6*) is used in the Level 3 processing to remove atmospheric muon events.

7.3.3 Rates at Level 3

The rates after the Level 3 cuts are applied is shown in Table 7.1. The atmospheric muons are reduced by about an order of magnitude. The removal of accidental triggered events forms a large part of the reduction in rate at Level 3, with the rates decreased by more 96%.

7.4 GRECO Level 4 Cuts

The first GRECO-specific cut level is designated *level 4*, or *L4*, was first introduced in 2011 using very similar variables at the Level 3 cuts. This is performed for historical reasons, as the DeepCore Level 3 and GRECO Level 4 were produced in parallel.

As in the DeepCore Level 3 processing, the GRECO Level 4 is divided into two types of cuts: those that remove accidental triggers due to detector noise and those that remove atmospheric muons. The cuts for atmospheric muons are then fed into a *boosted decision tree* (*BDT*), a multivariate algorithm designed to better separate signal from background [18].

7.4.1 Accidental Rejection at L4

Similar to the cuts applied at Level 3, the GRECO Level 4 begins with a cut on the number of observed hits. In this case, static time window cleaning is applied with a range of $-3500\text{ns} \leq t \leq 4000\text{ns}$ for hits in the DeepCore fiducial volume. A dynamic time window cleaning is then applied with a window of 200 ns. Any events with fewer than three hits in this stricter pulse series is removed.

7.4.2 Muon Rejection at L4

Some cuts used to identify muons in the GRECO Level 4 are similar to those applied in the Level 3 processing. A stricter hit cleaning algorithm is used at this cut level to identify muons missed at Level 3.

FirstHit Z

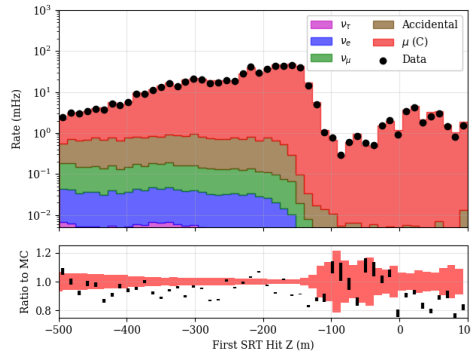


Figure 7.3 – The Z position of the first hit in a cleaned hit series. Note the shape difference between the atmospheric muons in red and the various neutrino flavors, particularly above -200 meters.

The Z position of the first hit DOM in the event is included for the GRECO Level4. The cut continues to show separation between neutrino events and atmospheric muons with the new hit cleaning.

NAbove200

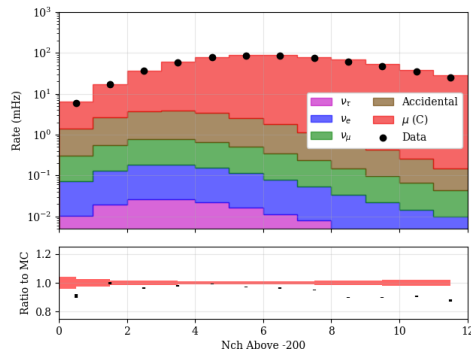


Figure 7.4 – The number of hits above Z=-200 meters

Similarly, the number of hit DOMs identified above Z=-200 m is again used with a new hit series. Once again, some separating power remains.

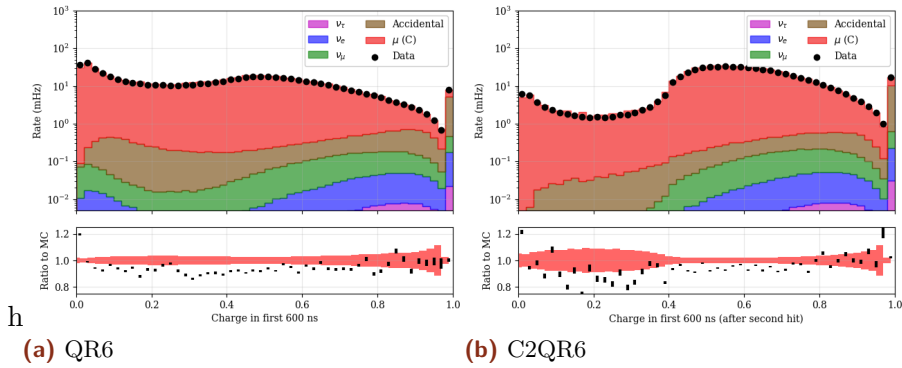


Figure 7.5 – The charge ratio variables used in the L4 cuts.

lofsubfigure\newline numberline(a)QR6lofsubfigure\newline numberline(b)C2QR6

QR6/C2QR6

Both the QR6 and C2QR6 are used in the GRECO Level 4 processing. The two show some degeneracy, although the BDT training suffers if only one is available. Note that there exists some significant disagreement between data and simulation at low values of C2QR6. This region does not contain much signal and will be removed by the BDT.

Tensor of Inertia

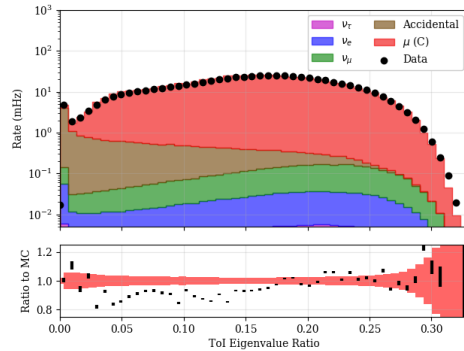


Figure 7.6 – The eigenvalue ratio from a ToI calculation. Larger values indicate more apparent elongation in the event.

At this early level, the shape difference in the observed hit pattern will be relatively clear. Many neutrinos with energies in the range of 1-100 GeV will appear to be rather small and compact in DeepCore forming a cascade-like event. Muons will have a longer visible track. These differences may be interpreted via use of the *Tensor of Inertia eigenvalue ratio* (more briefly, *ToI*). This variable is defined in analogously to the tensor of inertia from mechanics, with the measured charge taking the place of the mass.

$$\begin{aligned} I_X &= \sum_{i=0}^{nhits} (y_i^2 + z_i^2) q_i \\ I_Y &= \sum_{i=0}^{nhits} (x_i^2 + z_i^2) q_i \\ I_Z &= \sum_{i=0}^{nhits} (x_i^2 + y_i^2) q_i \end{aligned} \quad (7.5)$$

These three moments yield information about the shape of the event. The eigenvalue ratio is defined as

$$e = \frac{\max(I_j)}{I_x + I_y + I_z} \quad (7.6)$$

Events which are very track-like, and therefore muon-like, have eigenvalue ratios near 0 while more cascade-like events have eigenvalue ratios close to $\frac{1}{3}$.

Linefit Speed

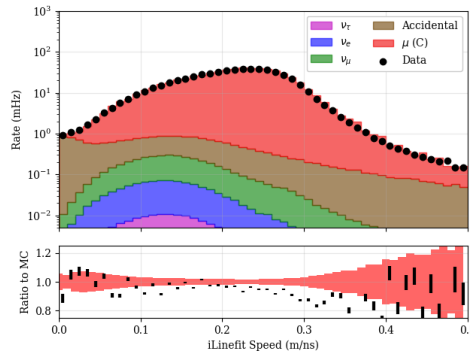


Figure 7.7 – The apparent speed, in units of meters per nanosecond, corresponding to the hits in the event. Faster speeds are associated with particle travel instead of light travel.

The *line fit* is a first-guess reconstruction used in IceCube. The algorithm assumes that the hit pattern in an event may be modeled as a plane wave passing through the detector at speed v_{LF} . The speed of the plane wave may be solved analytically [19].

$$\vec{v}_{LF} = \frac{\langle t_i \cdot \vec{x}_i \rangle - \langle \vec{x}_i \rangle \langle t_i \rangle}{\langle t^2 \rangle - \langle t_i \rangle^2} \quad (7.7)$$

where $\langle t_i \rangle$ denotes the average hit time. Cascade-like events have hits moving without a preferred direction while the atmospheric muons have a single preferred direction. Using the line fit speed, the neutrino sample is expected to have a speed closer to 0 while the atmospheric muons show a speed closer to the speed of light, 0.3 m/ns.

The L4 BDT

A Boosted Decision Tree (*BDT*) is trained at L4 to further reduce the atmospheric muon background by a factor of 10x. The variables described above were provided to a BDT training using the CORSIKA as the background training sample and GENIE simulation as the signal sample. The BDT uses a series of *trees*, collections of multidimensional cuts, to classify events as either signal-like or background-like [18]. After *boosting*, a process by which event weights are adjusted based on the success or failure of previous classification attempts. The BDT returns a *score* ranging from -1 (background-like) to +1 (signal-like) which may be used as a cut variable in an analysis.

The score returned by the GRECO Level 4 BDT is shown in Figure 7.8. The distribution ranges from -0.6 to +0.6, indicating that no signal or background events are perfectly identifiable. Separation is observed between the atmospheric muon events, which peak around a score of -0.25, and signal, peaking at +0.15.

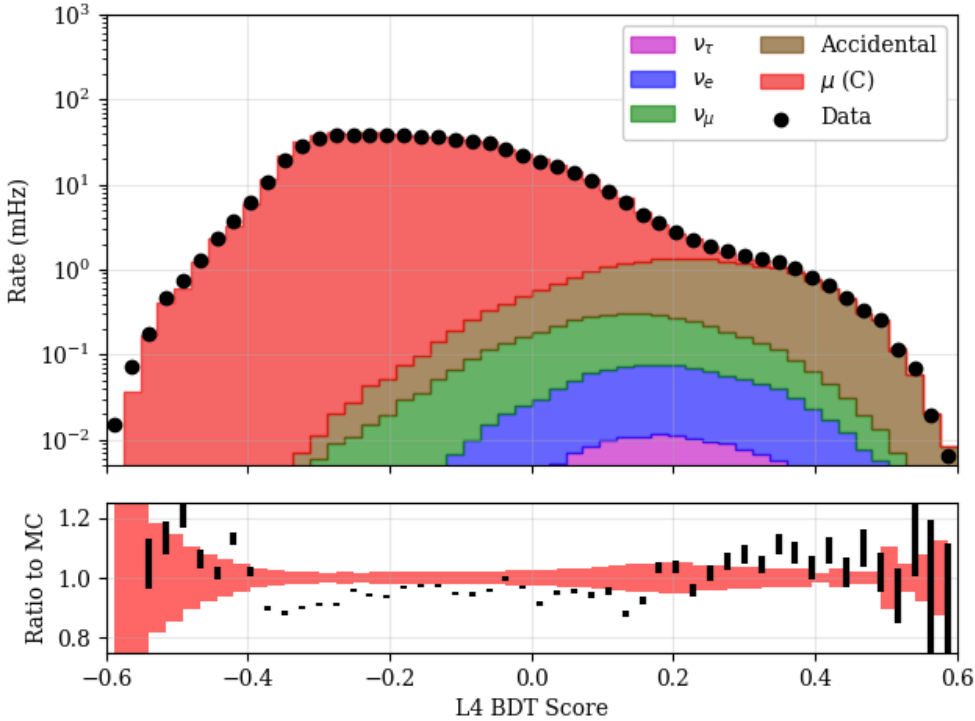


Figure 7.8 – The distribution of the boosted decision tree used at L4. A cut is applied at 0.04 to remove a significant fraction of atmospheric muon background events. Note the ratio, which shows disagreement in the very muon-like region. The region of disagreement is removed by the cut.

Comparisons to MC show mild disagreement, particularly in the most muon-like regions that get cut away. It's not obvious what causes the disagreement, although it is possible that the assumed cosmic ray flux model is simply an inaccurate model of some part of the spectrum that contributes. Alternatively, this may be an artifact of undiscovered mismodeling of the atmospheric muon events. Differences in the high energy muon events would likely have clear tracks visible in the detector, contributing to the region around -0.5. No investigation of the disagreement has been performed, as these events are removed from the GRECO selection.

A shoulder attributable to the accidental triggers is visible at high values of the BDT score, peaking around 0.25, indicating that these events appear more signal-like than the neutrino samples. While initially puzzling, investigation of the training of the BDT showed that the original training sample did not include these events. Instead, only CORSIKA and GENIE events were used to train the BDT. Because the training lacked any accidental triggers as a reference, the BDT picked the most obvious feature of the GENIE sets: that the signal events were primarily low energy with lower light deposition than the background. These are also key features of the noise triggers.

The GRECO Level 4 places a cut at 0.04 in the BDT score, removing a large fraction of the background sample. A large fraction of the neutrino sample is also removed in order to reduce the muon rates by a factor of 20x.

7.4.3 Rates at Level 4

The rates of the selection after the Level 4 cuts are applied is shown in Table 7.2. After the GRECO Level 4 BDT, the number of atmospheric muons is reduced to 50 Hz, a

Type	IceCube Processing			GRECO L4
	Any Filter	DC Filter	Low-en L3	
CORSIKA	990598	9178	969.818	50.511
MuonGun	60669	2982	442.493	33.562
Accidentals	35855	8117	283.559	11.963
ν_e	1.842	1.721	1.262	0.783
ν_μ	11.317	6.360	4.758	2.503
ν_τ	0.293	0.270	0.206	0.134
MC Total*	1026466	17303	1260	65.893
Data	1154426	19092	1092	68.592

Table 7.2 – The event rates after the Level 4 cuts in GRECO. The total simulated rate is calculated using CORSIKA events and ignoring MuonGun. The data rate is estimated from a burn sample of 30 runs at Level 4. Rates are given in mHz.

mere 25x the muon neutrino rate. The number of accidental triggers is also reduced in the analysis due to the dedicated cuts applied at this level. The number of accidental triggers is still larger than the number of neutrinos expected, however, indicating that further cuts are necessary.

7.5 GRECO Level 5 Cuts

The next stage of cuts, known as the *GRECO Level 5*, or more simply, *L5*, also uses a BDT.

7.5.1 Accidental Rejection at L5

Unlike the previous stages, however, there is no explicit cut introduced at L5 to remove accidental triggers. Instead, an implicit requirement on the number of hit DOMs arises due to the reconstruction used at Level 5. The STW+SRT pulse series containing DeepCore fiducial pulses is used to fit a total of 6 free parameters. The parameters are degenerate if fewer than five hits are used. In this case, the reconstruction fails to converge and the event is removed. Because of this degeneracy, the GRECO Level 5 implicitly requires at least 6 hit DOMs in this hit series.

7.5.2 Muon Rejection at L5

Time to 75% Charge

The first variable used to create the L5 BDT is the amount of time required to deposit 75% of the total charge, the t_{75} . Similar to the QR6 and C2QR6 variables, the t_{75} is a variable designed to look at the hit distribution in time. However, the variable is now produced in the reverse manner: where the QR6 variable refers to the amount of a charge in a given window, the t_{75} instead attempts to find the amount of time for a given charge level. This provides an on the total event length and timing distribution.

The neutrino events deposit energy quickly due to the low energies of the sample of interest in this thesis. The muon events take longer to reach 75% of the total charge due to the long travel time of the events through the detector.

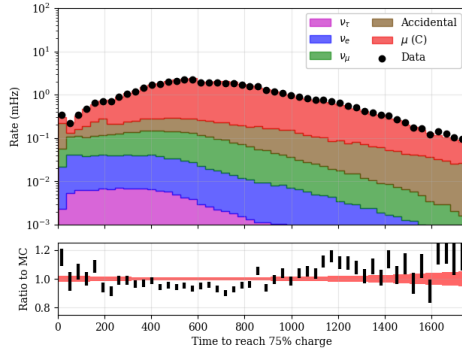


Figure 7.9 – The time to accumulate 75% of the total charge of the event.

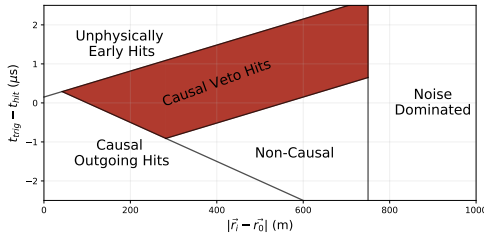


Figure 7.10 – A schematic diagram showing the regions of the VICH algorithm. VICH returns the number of hit DOMs in the shaded region, corresponding to the pulses that are both causally connected with the trigger and entering DeepCore.

Veto Identified Causal Hits

The *Veto Identified Causal Hits* (VICH) algorithm is also used in the GRECO Level 5. This algorithm uses an uncleared hit series to search for hits that are causally connected to the trigger [17]. The first DOM to contribute to the DeepCore trigger is used to define the trigger time and position.

Five regions are defined based on various criteria shown in Figure 7.10. Hits which are not causally connected to the trigger are ignored. Hits which occur too far away from DeepCore are also ignored to reduce the effect of detector noise. A causal region which is consistent with light travel outgoing from the trigger position is also ignored.

The VICH algorithm returns the number of hits in the remaining "causal veto region".

First Hit ρ

The Z position of the first hit was used in the GRECO Level 4 cuts in order to identify atmospheric muons coming from above DeepCore. The X and Y position may also be used to identify muons. These are combined to define a *radial distance* (ρ_{36}) from the center of DeepCore, here defined to be the position of string 36 at $(x, y) = (46.3, -34.9)$.

$$\rho_{36} = \sqrt{(x - x_0)^2 + (y - y_0)^2} \quad (7.8)$$

The radial distance is a general parameter and can be used with any event vertex. For the GRECO Level 5, the first hit in the STW+SRT pulse series is used. Atmospheric muons entering DeepCore are more likely to be found at larger values of ρ_{36} while neutrinos are more likely to be found within the DeepCore fiducial volume, which stops at $\rho_{36} = 125$.

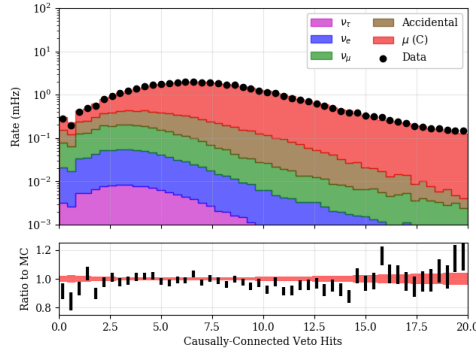


Figure 7.11 – The amount of causally-connected charge discovered in the veto region.

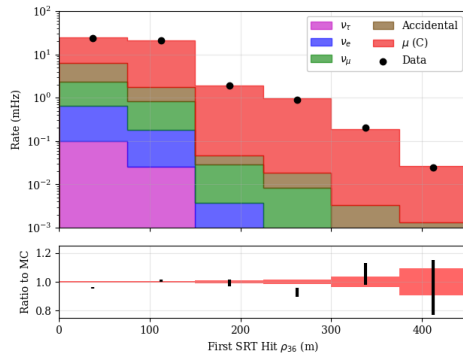


Figure 7.12 – The radial position of the earliest hit of a cleaned hit series. The radial position is measured relative to string 36, the center of DeepCore.

Quartiles CoG

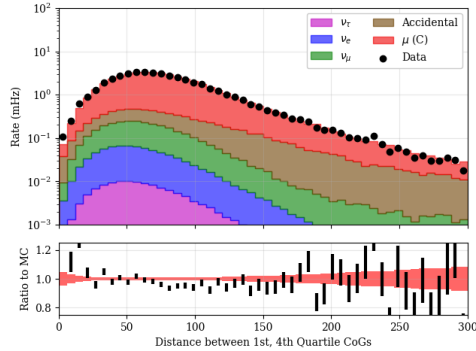


Figure 7.13 – The distance between the centers of gravity of the first and last quartile in time.

The distance traveled by muons may be exploited as well. In particular, a track-like event is expected to travel over a longer distance than a cascade-like event of a similar energy. In GRECO Level 5, the distance between the CoGs of the first and last quartiles in time are used to characterize the distance traveled by the interaction. For atmospheric muon events, this distance is expected to be larger than for low energy neutrino events.

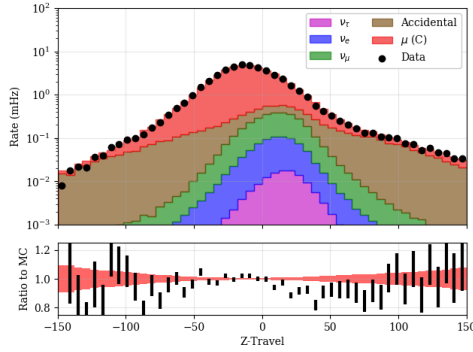


Figure 7.14 – The distance traveled in Z between the first and last quartile of hits in time.

Z-Travel

The total distance traveled in the detector is only one useful measure that may be calculated using the quantiles in time. Another useful metric is the distance traveled only in the Z coordinate. The value, known as the *z-travel*, is a measure of the direction of the particle

$$\Delta Z = Z_{Last} - Z_{First} \quad (7.9)$$

The z-travel is typically used to identify atmospheric muons. Atmospheric muons traveling through the detector from above will have a negative z-travel distance and neutrinos may be positive or negative, but is likely to be small due to the small size of neutrino events. The accidental triggers also are also well-separated from the simulated neutrinos. These events do not have a preferred direction and appear at all values of the z-travel and appear at all values. The accidental events dominate at the tails of the distribution.

SPE Zenith

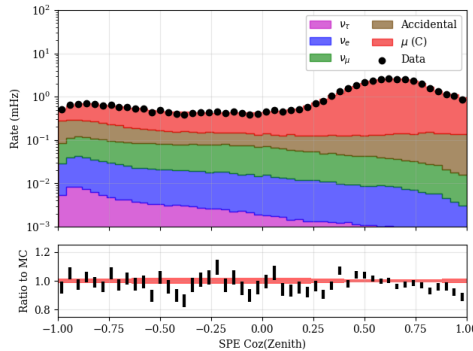


Figure 7.15 – The zenith angle distribution of events from an 11-iteration SPE fit. The fit assumes an infinite track hypothesis and uses only hit DOMs.

More advanced reconstructions are viable at this level, providing new potential for the identification of atmospheric muons from neutrino candidates. These reconstructions must account for the effects of scattering in order to produce meaningful results.

The time required for a Cherenkov photon to reach a DOM from a point-like emission is

$$t_{point} = t_{emission} + \frac{n}{c} |\vec{r}| \quad (7.10)$$

where $|\vec{r}|$ is the distance between the emission point and the DOM. The corresponding time from a muon track is

$$t_{track} = t_{emission} + \frac{\vec{r} \cdot \hat{n} + \rho \tan \theta_C}{c} \quad (7.11)$$

where \hat{n} is a unit vector pointing in the direction of the muon track, θ_C is the Cherenkov angle, and $\rho = |\vec{r} - (\vec{r} \cdot \hat{n}) \hat{n}|$ is the impact parameter of the track with respect to the DOM [11]. In the absence of scattering, all photons would arrive at the DOM according to these times. The addition of scattering delays photons, as they travel a greater distance before reaching the DOM. These delayed photons give a *time residual* distribution.

There is no analytic form for the timing which includes the effects of scattering, although approximations exist. One such approximation, the Podel function [20], may be used to estimate the time residual distributions as a function of source-reciever distances [21].

The Podel functions may be used to construct a likelihood of the form

$$L(x_{vertex}, t_{vertex}, \hat{n}) = \prod_i^{pulses} \frac{dP_{Podel}(t_i - t_{point} | x_{vertex}, t_{vertex}, \hat{n})}{dt} \quad (7.12)$$

where P_{Podel} the Podel function used to model the distribution of time residuals. This likelihood may be maximized or, equivalently, the negative log-likelihood may be minimized in order to obtain the best-fit values for the position, time, and direction of the track. The likelihood construction assumes an infinite muon track without defined starting and stopping points. Because this construction implicitly assumes that only one photon is received per DOM, this is referred to as the *single photoelectron (SPE)* fit.

The SPE fit is minimized numerically using the simplex method [22]. A total of 11 seeds are used for the SPE fit performed in the GRECO Level 5, each of which differs from the others in direction. A minimization is performed with each seed and the best fit result is returned. The GRECO Level 5 SPE fit uses another SPE fit, performed with only 2 seeds produced during the general IceCube processing at Level 2.

The zenith angle returned by the SPE fit is used in the Level 5 processing. The atmospheric muons are primarily downgoing events. Therefore the direction of the reconstructed track is a useful tool for separating neutrino signal and atmospheric muon background.

The L5 BDT

The six variables described in the GRECO Level 5 are again used to train a BDT. At the time of training, updated versions of both the GENIE and CORSIKA simulations were provided as part of a ongoing upgrade of the IceCube simulation. The L5 BDT was trained using simulation files containing the then-newly available Vuvuzela V1 noise model and an updated version of the GENIE Monte Carlo generator.

A set of fifteen variables were tested. At each step of the training, the least important variable was removed to limit the possible effects of overtraining. The process continued until changes in the cut efficiency larger than 1% were observed, resulting in a boost decision tree containing the six most important variables tested as described above.

The distribution of BDT score is shown in ???. The data and simulation show good agreement in the muon-dominated region. In the signal region, the data statistics is low,

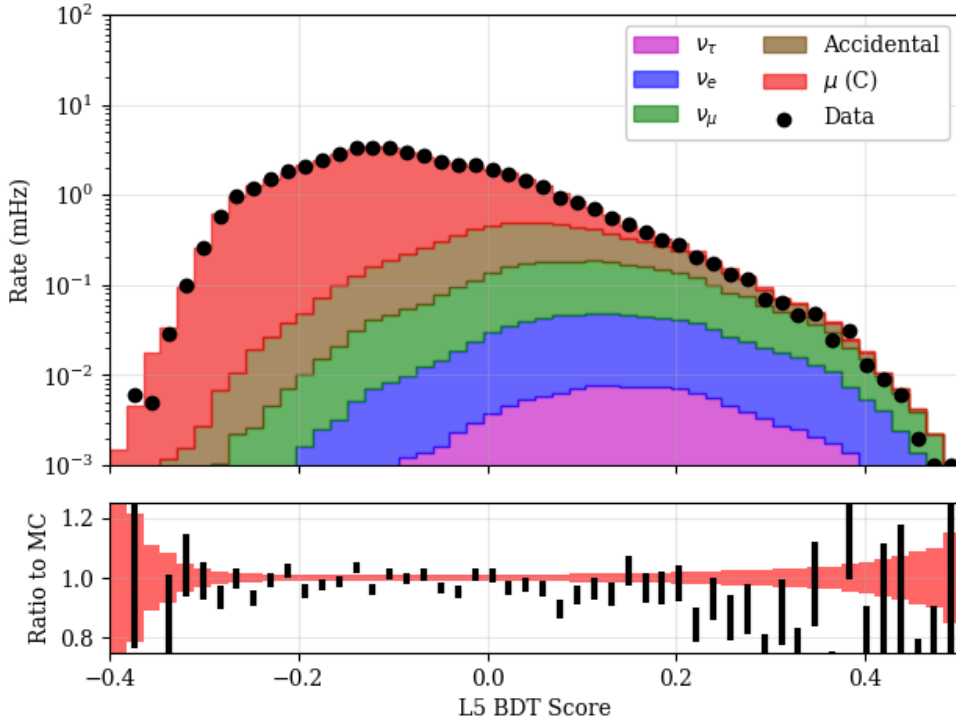


Figure 7.16 – The distribution of the boosted decision tree used at L5. A cut is again applied at 0.04 to remove a significant fraction of atmospheric muon background events.

but the rates are consistent between data and simulation. A cut is placed at a score of 0.04, which gives approximately 95% background rejection with a somewhat significant hit of 30% to all neutrino rates.

7.5.3 Rates at Level 5

After the GRECO Level 5 cuts, the event rates for the atmospheric muons are a factor of 3x larger than the neutrino flux. The rate from accidental triggers in the detector is comparable to the muon neutrino rate. The tau neutrino rate is more than an order of magnitude smaller than the muon rates, making up less than 2% of the total rate. Additional cuts are needed in order to lower both sets of background below the neutrino rate.

7.6 GRECO Level 6 Cuts

Unlike previous levels, the GRECO L6 does not rely on a trained boosted decision tree. The choice was made due to concerns about the significantly limited background simulation. Such a limitation could lead to overtraining, a situation difficult to test with few simulated events.

Two cuts are applied to the sample at GRECO Level 6 for the removal of the remaining accidental triggers. An additional three cuts are applied to reduce the muon background rate.

7.6.1 Accidental Rejection at L6

Type	IceCube Processing			GRECO	
	Any Filter	DC Filter	Low-en L3	L4	L5
CORSIKA	990598	9178	969.818	50.511	4.100
MuonGun	60669	2982	442.493	33.562	3.022
Accidentals	35855	8117	283.559	11.963	1.799
ν_e	1.842	1.721	1.262	0.783	0.544
ν_μ	11.317	6.360	4.758	2.503	1.629
ν_τ	0.293	0.270	0.206	0.134	0.103
MC Total*	1026466	17303	1260	65.893	8.176
Data	1154426	19092	1092	68.592	7.422

Table 7.3 – The event rates after the Level 5 cuts in GRECO. The total simulated rate is calculated using CORSIKA events and ignoring MuonGun. The data rate is estimated from a burn sample of 30 runs at Level 5. Rates are given in mHz.

Fill-Ratio at L6

After GRECO Level 5, the accidental trigger rate is significantly larger than the expected rate of neutrinos. While the rate of these accidental triggers is low at this stage relative to the rate at L3, they form an important background to the remaining set of neutrino events. In order to limit their effect, two cuts are introduced to separate signal neutrinos from the accidental background.

The first of these cuts, the *fill-ratio*, is a variable typically used in the search for high energy cascades [23, 24] by quantifying the topology and compactness of hits within an event.

Fill-Ratio begins with a reconstructed vertex and pulse series. In the case of the GRECO Level 6, the first hit position in DeepCore within a STW+SRT cleaned pulse series is used as an event vertex. Both the pulse series and the event vertex are used in the fill-ratio calculation.

A radius is computed using the provided information. Many options are available for the calculation of different radii, including calculations using the mean or variance of the distance between the pulses and the vertex, a parametrized radius calculation using the number of hit DOMs, and a calculation using a previously reconstructed energy. Each configuration was tested in GRECO Level 6 with the calculation using the mean distance from the vertex showing the most promise.

$$\bar{r}_{\text{Fill-Ratio}} = A \left| \frac{\sum_i^{npulses} (\vec{x}_i - \vec{x}_{\text{vertex}})}{npulses} \right| \quad (7.13)$$

where A is a configurable scale factor. The algorithm next identifies all DOMs contained within a sphere centered on the provided vertex with a radius of $\bar{r}_{\text{Fill-Ratio}}$. The fill-ratio value is then given by the ratio of contained DOMs observing a pulse to the total number of contained DOMs.

$$f = \frac{\sum_i^{ncont} (|\vec{r}_i| < \bar{r}_{\text{Fill-Ratio}} \& Q_i > 0)}{\sum_j^{ncont} (|\vec{r}_j| < \bar{r}_{\text{Fill-Ratio}})} \quad (7.14)$$

This results in a measure of the compactness of a hypothetical cascade, where we expect the resulting hit distribution to be approximately spherically symmetric. An approximately spherically symmetric cascade-like event will completely fill the fill-ratio

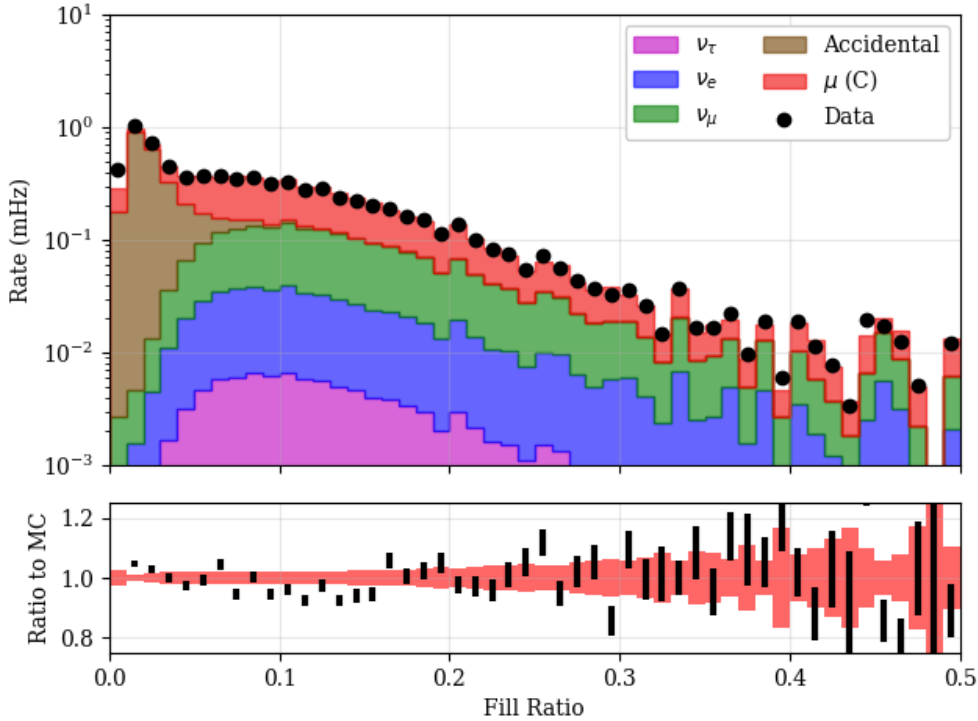


Figure 7.17 – The fill-ratio distribution. Note the excess of events at low values, a region dominated by the accidental triggers due to detector noise in simulation. A cut is applied at 0.05 to remove these accidental triggers.

sphere, resulting in a value near 1.0. An extended, track-like event will have hits that are, on average, further from the starting vertex, leading to a large value of $\bar{f}_{FillRatio}$, a large number of contained DOMs, and a small value of the fill-ratio.

In the context of high energy events, the fill-ratio provides good separation between cascade-like and track-like events. Fill-ratio has not previously been used in low energy analyses, however, due to the short muon tracks of muon neutrino interactions in the 20 GeV region important for atmospheric oscillations. At GRECO Level 6, fill-ratio has been tested to identify neutrino and atmospheric muon events with no significant separating power observed.

Significant separating power was observed between the neutrino events and accidental triggers, however. The accidental triggers include pulses throughout the detector with no clustering in the event, unlike events caused by muon or neutrino interactions, which typically have some type of clustering of pulses around the interaction position. These events receive a large radius due to this lack of clustering and a correspondingly small value of the fill-ratio. A choice of $A=1.6$ and the radius calculated using the mean distance between the first hit and all other cleaned pulses gives the separating power shown in Figure 7.17.

The observed separation at a value of 0.05 allows up to one order of magnitude of reduction in the rate of accidental triggers with a relatively small reduction in signal rate of approximately 10%. The use of fill-ratio reduces the number of accidental triggers expected below the neutrino rate.

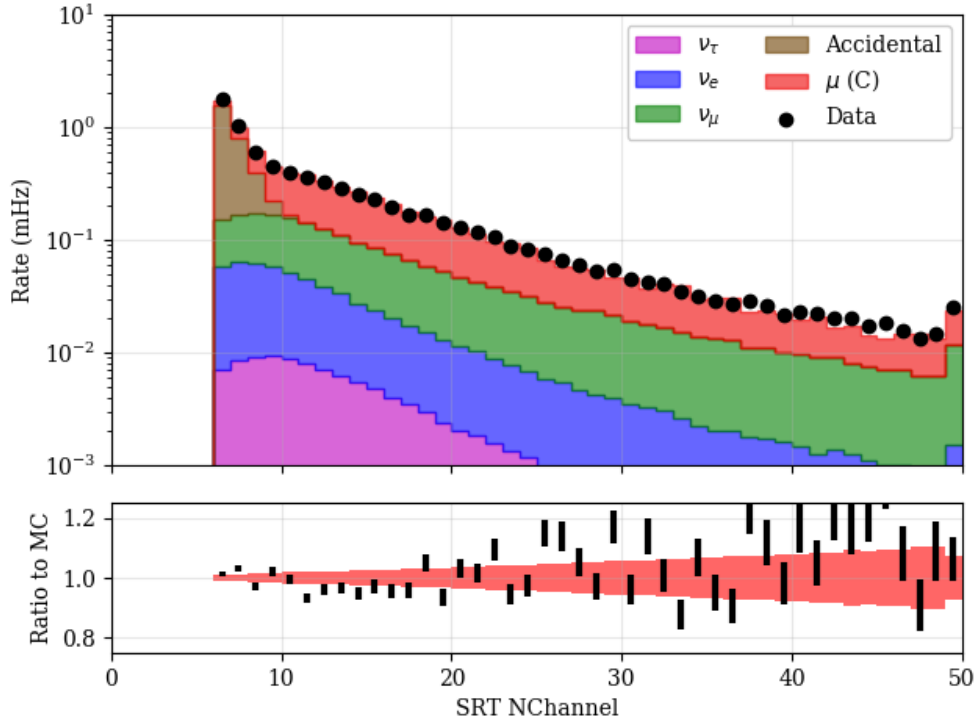


Figure 7.18 – The number of channels in the STW+SRT cleaned hit series at GRECO Level 6. At least 8 hits are required for the reconstruction performed at GRECO Level 7. Events with fewer than 8 hits are removed during Level 6, coincidentally reducing the number of accidental triggers expected.

The L6 NChannel Cut

At GRECO Level 5, the SPE reconstruction was used to calculate the position, time, and direction of an infinite muon track. The final reconstruction used in this analysis, Pegleg, is discussed in Section 7.7. Like the SPE reconstruction used at Level 5, the Pegleg reconstruction requires a minimum number of hits in order to converge. In order to prepare for the reconstruction performed at GRECO Level 7, events with fewer than 8 hits in the STW+SRT cleaned DeepCore pulse series are removed from the selection. This removal is performed in order to prepare for the Pegleg reconstruction, but it also removes a significant number of accidental triggers from the selection. These events, shown in Figure 7.18, The accidental triggers make up about 0.3% of events in the sample following the combination of this cut as and the fill-ratio cut.

7.6.2 Muon Rejection at L6

CorridorCut

The remaining atmospheric muon background after the GRECO Level 5 processing show strong selection bias, with few events remaining showing clear tracks in the veto region. In the past, minimum-ionizing muons were discovered to be leaking into the DeepCore fiducial volume along *corridors*, lines connecting the inner part of the detector to the outer edge without crossing any strings. These events pass between strings and leave little trace in the form of identifiable hits in the outer detector. Examples of these corridors are shown in Figure 7.20.

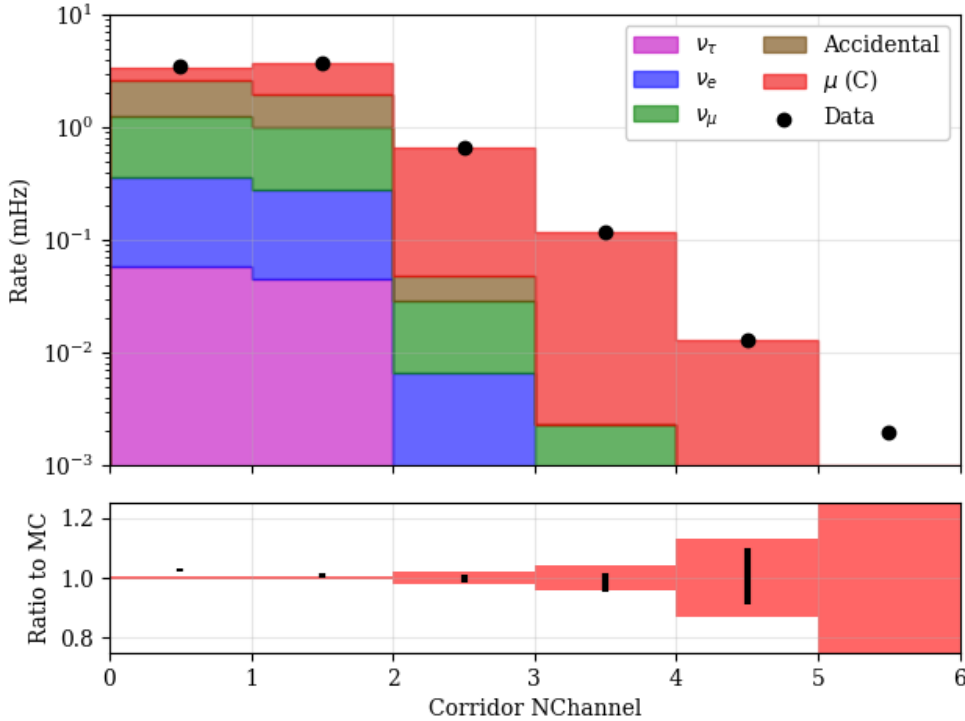


Figure 7.19 – The number of channels discovered along one of the various "corridors" in the detector. Events with at least two hits discovered along a corridor are removed.

In order to identify these muons, a cut was developed to look along pre-defined corridors for SLC hits correlated with pulses in DeepCore. A CoG of the event is calculated from the STW+SRT cleaned DeepCore pulse series. The string nearest the CoG is used to choose a set of 'corridor' strings to check for the event. The number of hit DOMs found on the corridor strings in an uncleaned pulse series is returned.

Due to the effects of random detector noise, a cut limiting the number of discovered corridor hits to 0 would result in a significant loss of signal events. Instead, one hit is allowed, with two or more discovered DOMs leading to the removal of the event from further processing. At this stage, there are few events due to atmospheric muons with detectable energy in the veto, resulting in the removal of few events. The events removed, however, are dominated by atmospheric muons, as seen in Figure 7.19.

FiniteReco Starting Containment

The SPE reconstruction used in L5 was created using an infinite muon hypothesis. In order to refine this reconstruction, the *FiniteReco* algorithm is employed.

FiniteReco is a module that accepts a previous reconstruction and a given set of pulses [17]. The start and end point of the muon track may be estimated by assuming light is emitted from the track at the Cherenkov angle. The direction of the muon track remains unchanged. In the GRECO Level 6 processing, the SPE reconstruction from the Level 5 processing is used in the FiniteReco reconstruction.

The starting position of the resulting reconstructed particle may be used to estimate the interaction point of the particle. Figure ?? shows the position of the reconstructed vertex in terms of depth and distance from string 36. If an event begins outside of the DeepCore fiducial volume, the event is likely to contain a muon and can be removed from

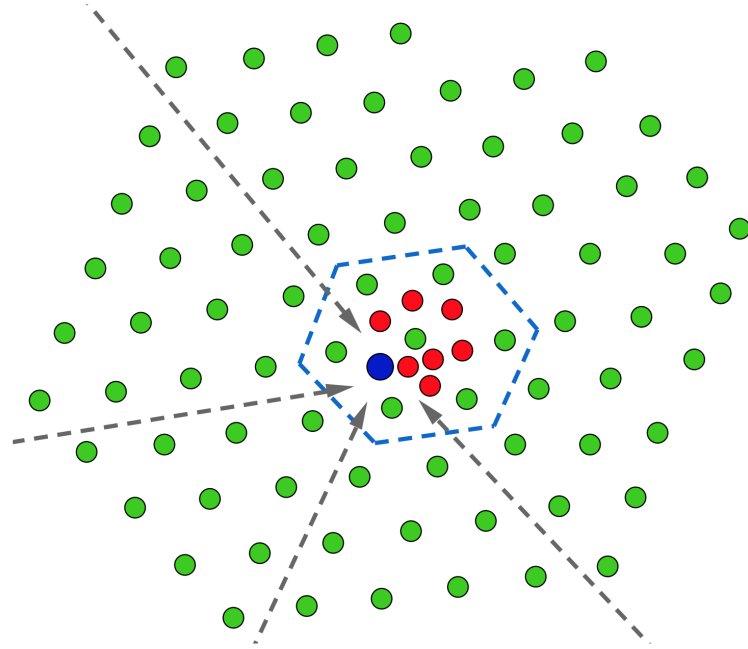


Figure 7.20 – An example of "corridors" into the DeepCore fiducial volume. Muons may pass into the fiducial volume, outlined in blue, undetected by following the paths indicated by the dashed lines. Image from [25]

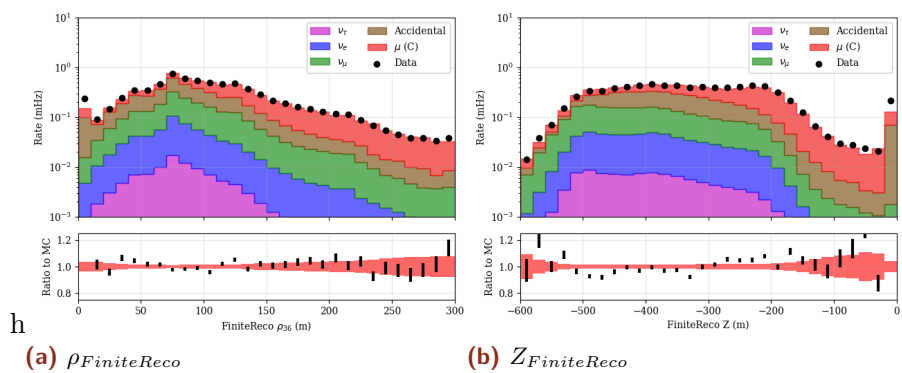


Figure 7.21 – The FiniteReco containment cuts. Note the excess of muons at the top and outer edge of the DeepCore fiducial volume.

lofsubfigure\newline(a)\rho_{FiniteReco}\newline(b)\newlineZ_{FiniteReco}

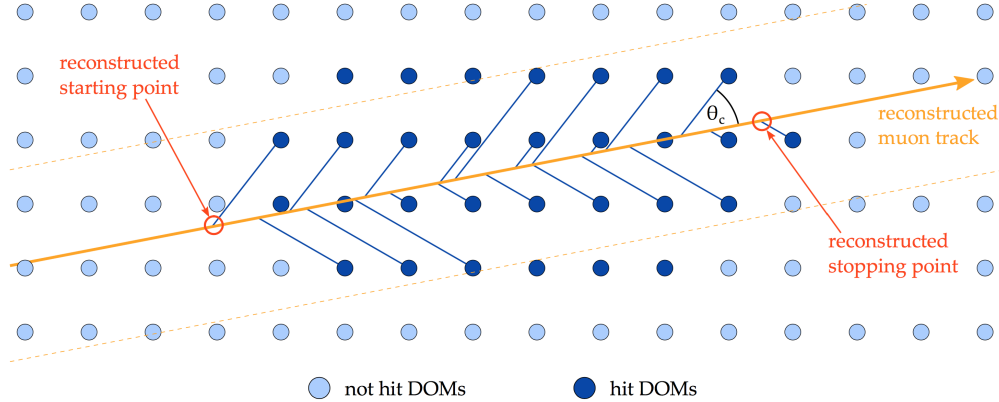


Figure 7.22 – The FiniteReco starting and endpoint reconstruction method. FiniteReco uses an existing muon track reconstruction and the collection of hit DOMs to estimate the starting and end point of the muon track. Diagram from [17].

the sample. Cuts are applied at the positions shown, resulting in a significant reduction in the number of muon events expected at final level.

7.6.3 Rates at Level 6

After the GRECO Level 6 cuts, the sample is dominated by neutrino events. The expected muon rate from CORSIKA simulation makes up 22% of the total sample. The rate from accidental events is also small, with only 5% of events due to random detector noise.

7.7 GRECO Level 7: Final Level

The final level of the GRECO event selection, *GRECO Level 7*, is the most computationally expensive stage of the selection. While previous stages have focused on speed, using cuts based on analytic variables or on fast reconstructions using approximations to the scattering of the ice, the GRECO Level 7 employs the Pegleg reconstruction. This reconstruction is expensive, requiring an average of 10 minutes per event.

The Pegleg reconstruction can be used to define new cuts to further reduce the atmospheric muon rates

7.7.1 Reconstruction using PegLeg

The existing reconstructions used in previous levels of the GRECO processing use either analytic or simplified likelihood reconstructions to estimate particle parameters. The position of the first hit and the finite muon reconstruction from FiniteReco provide separating power between atmospheric muons and neutrino events, but are designed to be computationally inexpensive instead of precise. At final level, these estimates are refined using a novel reconstruction method developed specifically for low-energy and oscillation searches with DeepCore.

The *PegLeg* reconstruction [13], a refinement of previous work [25], is a low-energy reconstruction that uses a hybrid cascade+muon hypothesis. The reconstruction returns a total of eight parameters: the position (x_R, y_R, z_R), time (t_R), direction (θ, ϕ), total energy (E_R) and track length (L_R). The algorithm requires seeds for each of the particle parameters and a collection of hits over which to run. Pegleg also requires a set of splines describing the expected charge as a function of distance from the emission point. These

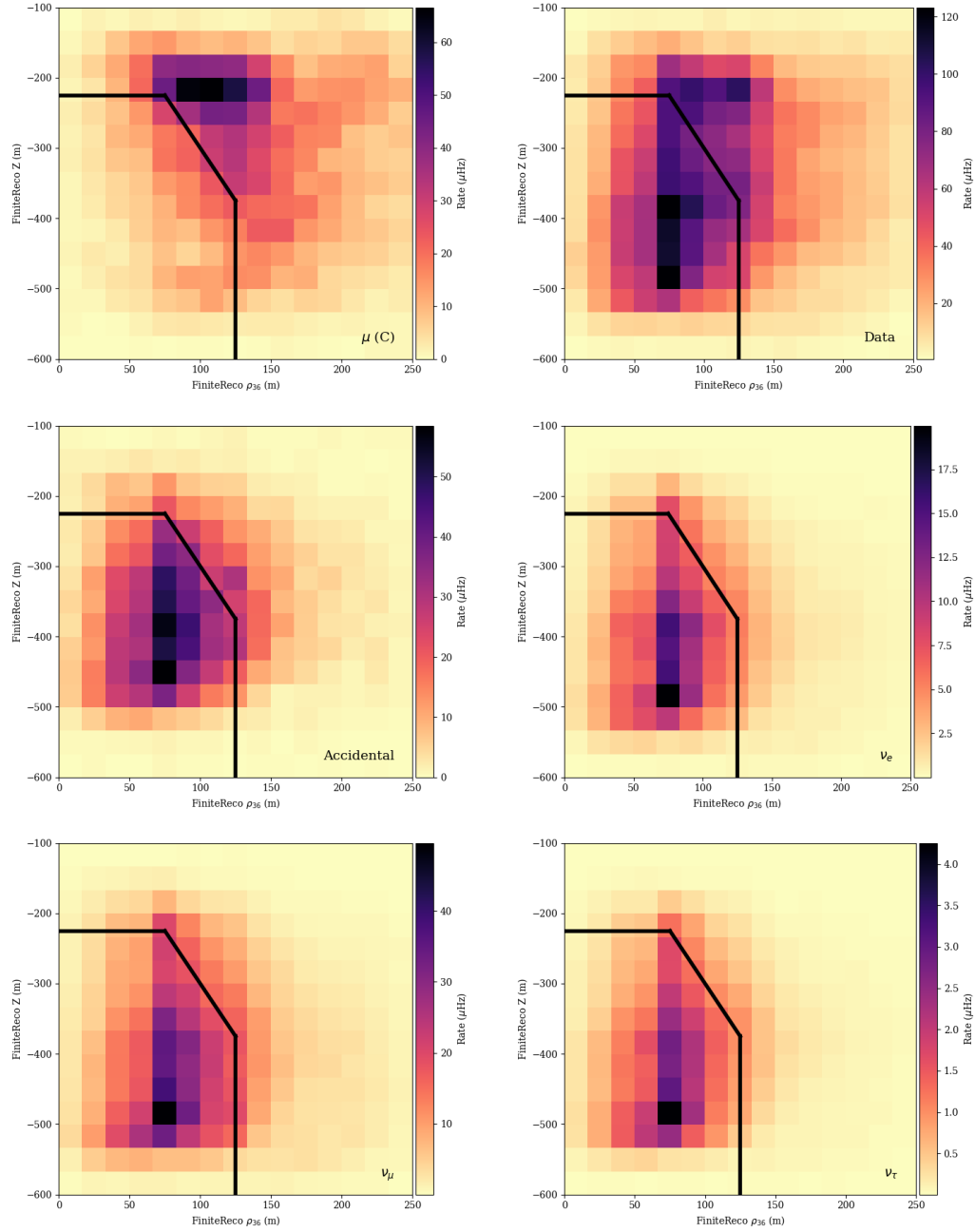


Table 7.4 – The FiniteReco containment cut for each of the channels. The cut itself is shown with the black line. The atmospheric muons, modeled with the CORSIKA generator, are reconstructed at the top of the DeepCore volume.

Type	IceCube Processing			GRECO		
	Any Filter	DC Filter	Low-en L3	L4	L5	L6
CORSIKA	990598	9178	969.818	50.511	4.100	0.443
MuonGun	60669	2982	442.493	33.562	3.022	0.315
Accidentals	35855	8117	283.559	11.963	1.799	0.102
ν_e	1.842	1.721	1.262	0.783	0.544	0.362
ν_μ	11.317	6.360	4.758	2.503	1.629	1.011
ν_τ	0.293	0.270	0.206	0.134	0.103	0.074
MC Total*	1026466	17303	1260	65.893	8.176	1.991
Data	1154426	19092	1092	68.592	7.422	1.841

Table 7.5 – The event rates after the Level 6 cuts in GRECO. The total simulated rate is calculated using CORSIKA events and ignoring MuonGun. The data rate is estimated from a burn sample of 100 runs at Level 6. Rates are given in mHz.

splines are created using the CLSim module (see Section 4.2.2) to directly account for the scattering and absorption properties of the bulk ice model.

For each particle hypothesis, the event is broken into time steps in time based on the observed pulses in the event. At each time step, the expected charge at each DOM is calculated based on the energy and position of the particle hypothesis. The charge expectation is evaluated for all DOMs, regardless of whether a hit is observed or not. The total likelihood of the hypothesis is then the product of the likelihoods at each DOM.

The likelihood space itself typically possesses multiple local minima due to the small number of hits. The fit is performed using the MultiNest minimizer package [26] in order to handle the complex likelihood space. The MultiNest algorithm calculates the likelihood for a set of 100 hypotheses at each iteration. The likelihood at each point is used to estimate the underlying likelihood space and produces new hypotheses for testing using importance nested sampling [27].

Given the large dimensionality of the space, significant computational power is required for the fit. Simplifications are introduced to reduce the computational requirements of the Pegleg reconstruction. Track lengths are limited to integer multiples of the track length used to produce the ice model spline functions. While this requirement is lifted in newer versions of the software [13], that change has not yet propagated to the current GRECO events. In addition, only DOMs within 150 meters of the current particle position are evaluated to find the expected charge. All other DOMs are assumed to have an expected charge consistent with noise rates. This assumption allows the minimizer to avoid costly calculations of expected charge for distant DOMs at the expense of higher energy event resolutions.

In early versions of the PegLeg fit, the charge of individual pulses is used directly in the likelihood calculations [28]. Following the discoveries discussed in 7.8.1, however, the use of the charge was removed [13]. In the version of PegLeg used in the final version of this analysis, a deadtime window of 45 nanoseconds is introduced for each DOM directly following a pulse. During this window, the DOM may not contribute any further information to the fit. This changes the reconstruction likelihood from being on the observed charge to being sensitive only to the observation or absence of charge. Using this modification, disagreements between the data and simulated pulses resulting from mismodeling may be minimized.

Each event takes approximately 10 minutes on average to converge in the reconstruction. There also exists a significant tail to the reconstruction time, sometimes extending to multiple hours for a single event. With a large expected sample of events, the reconstruction time is the most computationally intensive part of the event selection.

7.7.2 Containment with PegLeg

With a more refined reconstruction, additional constraints on the containment of the starting vertices are possible. Similar to the work done with FiniteReco at Level 6, the reconstructed Z and ρ_{36} receive cuts in two dimensions as shown in ???. Once again, events at the top of and near the edge of DeepCore are more likely to be muons. An additional cut is applied at the bottom of the detector in order to limit the effect of observed discrepancies between data and simulation. Removing these events results in a 75% reduction of the atmospheric muon background at a cost of approximately 10% of the overall neutrino rate.

7.7.3 Other Cuts at L7

Cuts are also applied to the average reconstructed energy per hit DOM (??) and the scatter in the timing distribution of hits (??). The former is expected to yield high values for events dominated by flaring DOMs (Section 7.7.3) or events where a particle interaction occurs very close to the face of a DOM. The distribution also shows some disagreement at low values, although good agreement between data and simulation is found for large values.

The reason for this is likely related to the issues discovered in 7.8.1, although this disagreement has not been investigated further. A cut removing events with more than 3 GeV/DOM is applied only to events with fewer than 14 hits, limiting the impact on the neutrino signal events.

The scatter in the hit times shows very good agreement between data and simulation and is useful as a proxy for the overall scattering of the event. The cut, which removes events where the standard deviation of the hit times is larger than 800 nanoseconds, is also only applied for events with fewer than 14 hits. This limits the loss of neutrino events while removing a fraction of the remaining accidental triggers.

The cuts applied to the standard deviation in the hit times and the reconstructed energy per hit DOM are applied in two dimensions, as shown in Figure ??.

7.8 Calibration Discoveries with GRECO

Checks with the GRECO selection during the search for appearance uncovered disagreements between data and simulation. Five discoveries made with the selection are discussed here.

7.8.1 The Simulation SPE Templates

During the development of the GRECO selection, new calibration measurements showed that the SPE peak in data was misaligned. This SPE peak, a part of the SPE template described for simulation in Section 4.3.1, is used to convert between the pulses of the waveform, in units of millivolts, and the charge units in IceCube, in units of photoelectrons.

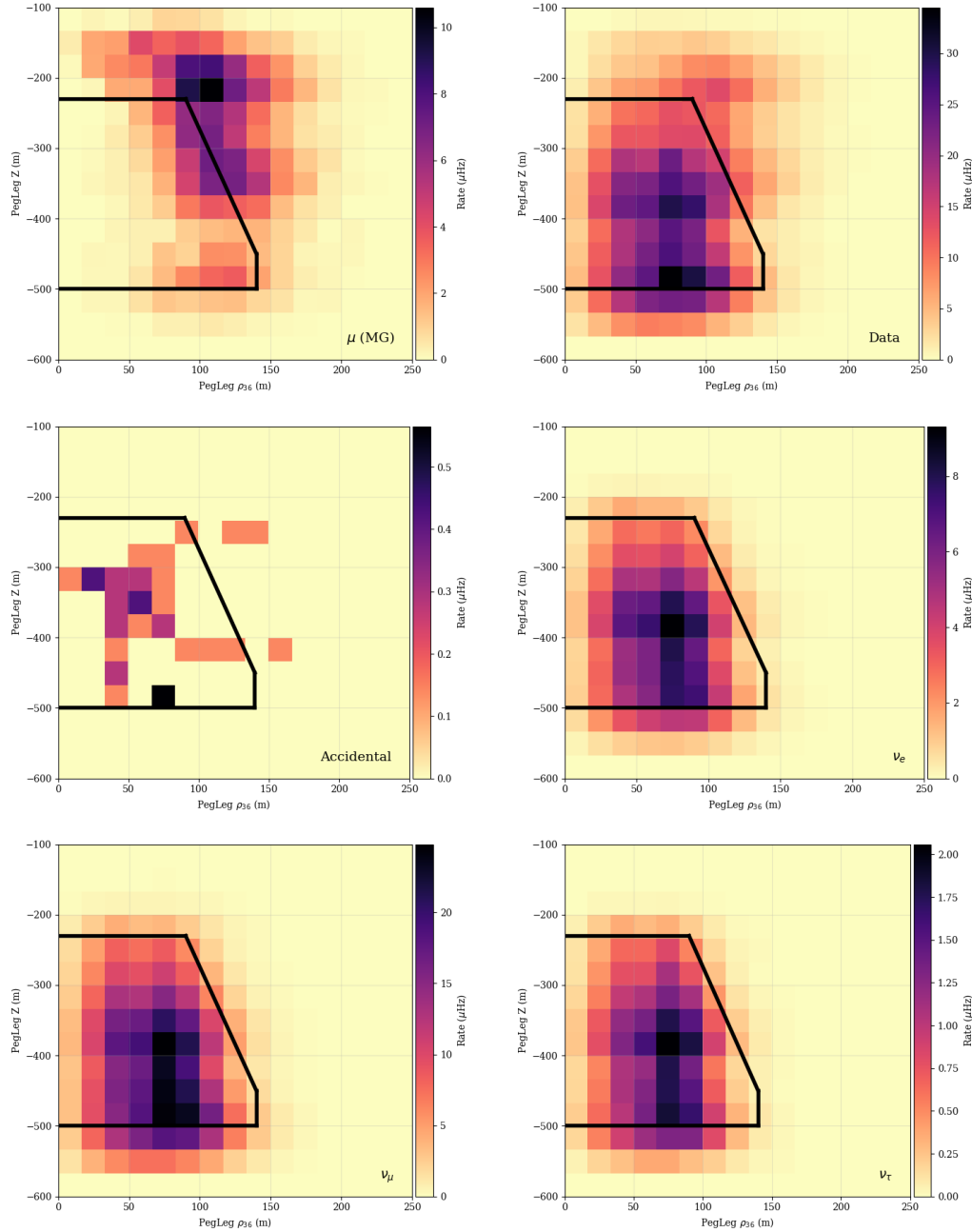


Table 7.6 – The Pegeg L7 containment cut for each of the channels. The cut itself is shown with the black line. Note that the atmospheric muons are here represented by the higher-statistics MuonGun sample.

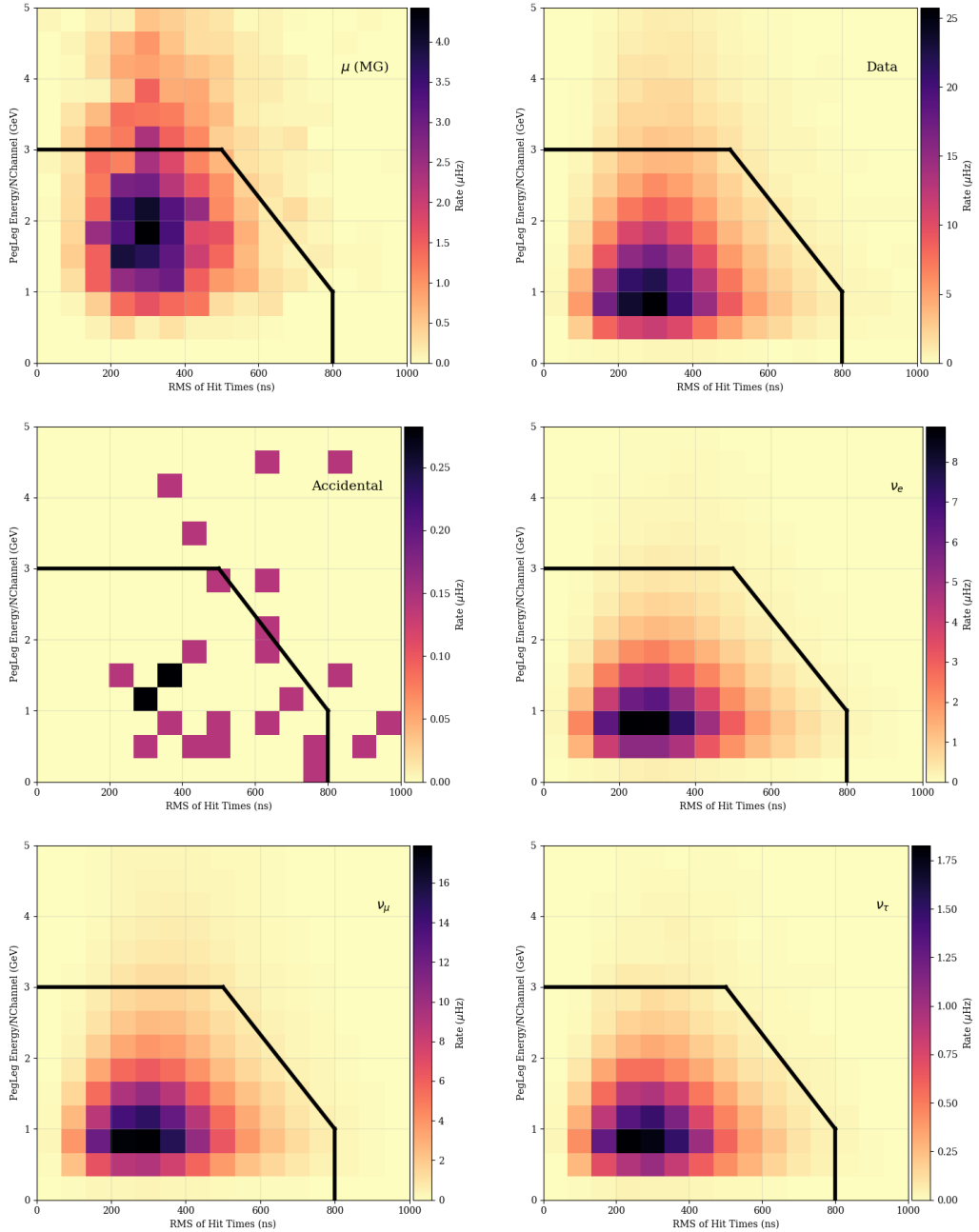


Table 7.7 – The cuts applied to the reconstructed energy per hit DOM and the standard deviation in the hit times. The cuts are designed to remove atmospheric muons and highly scattered hits from the selection. The 2D cut shown here is applied only to hits events with fewer than 14 hit DOMs.

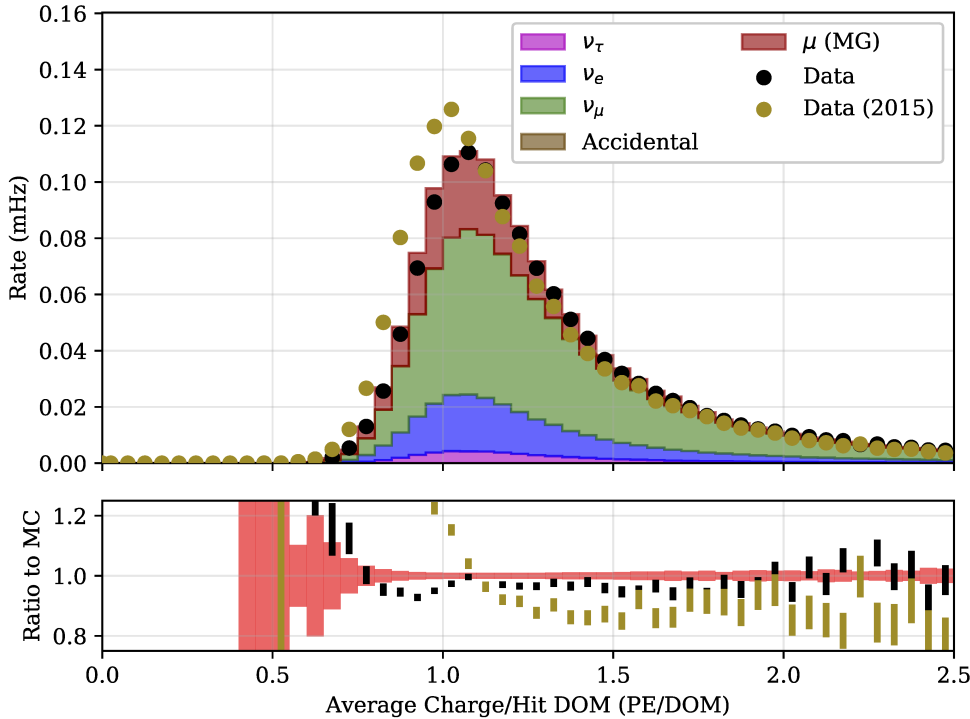


Figure 7.23 – The effects of the SPE correction applied to data in 2015. As expected, the peak of the distribution is closer to 1 PE in the corrected 2015 data (gold circles) than in previous years (black circles). The corrected data disagrees with the simulation.

The peak is intended to correspond to a value of 1 PE, indicating a single photon interacting at the photocathode of the PMT. While previous measurements had measured an average SPE template for the detector data, the new calibrations were used to measure the templates for individual DOMs.

The updated calibration measurements showed that the SPE peak used in data was not at 1 PE, but was, on average, at 1.045 PE. The IceCube collaboration subsequently corrected the SPE templates for data beginning in the IC86-5 (2015-2016) season, shifting the location of the extracted SPE peak in data from 1.045 PE to 1 PE. The correction is believed to result in a more accurate extraction of the charge in data. The simulation SPE template, shown in Figure 4.3, peaked at 1 PE by definition and was not changed. This shift mirrors effects observed during the fitting of the Vuvuzela V2 model in which a charge scaling variable was introduced to improve agreement with data and simulation (see Section 5.3).

After the correction, analyses searching for high energy neutrinos in the IceCube detector showed improved data and simulation agreement. Previous analyses searching for oscillations in DeepCore had observed good agreement between data and Monte Carlo simulations prior to the correction to the SPE template in data [IceCube-Oscillations2013, IceCube-Oscillations2015, IceCube-Oscillations2018]. In order to evaluate the effect of the correction, the IC86-5 data was processed using the standard GRECO processing scripts.

At low energies, most observed hits are due to single photons reaching the PMT. The average charge per DOM is therefore expected to approximately follow the SPE template.

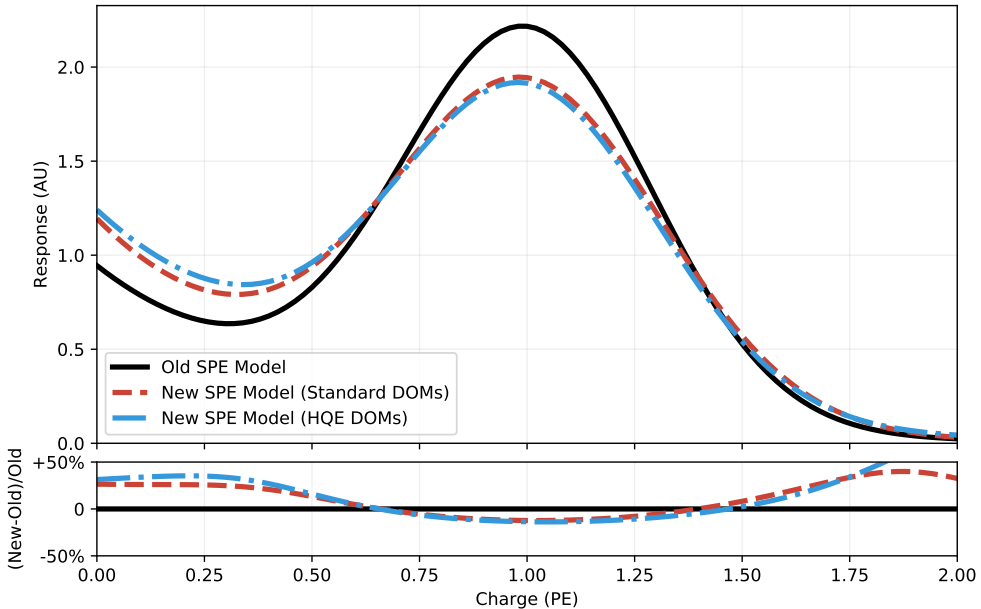


Figure 7.24 – A comparison of the old SPE template previously used in the simulation of events to the new average templates for the high quantum efficiency DOMs and the standard IceCube DOMs. The new models predict a higher number of pulses with low charge, consistent with the excess observed from the corrected 2015 data in Figure 7.23.

This variable was used to evaluate the effects of the correction at Level 7 of the GRECO selection.

The result is shown in Figure 7.23. As expected, the 2015 data shows a shift downward, with a peak closer to 1 PE. Unexpectedly, however, the corrected dataset shows substantial disagreement with simulated events.

Investigations of the disagreement showed that the data and simulation disagreed at all cut levels, including low cut levels unrelated to the GRECO selection. The issue has been identified to be the SPE templates used in the simulation. The template used is calculated as the average of the templates 118 DOMs measured in the lab prior to deployment [29]. All DOMs are simulated using identical parameters.

New work has been performed to apply the SPE templates measured in the data calibrations to the Monte Carlo simulation used in IceCube. These results have produced new SPE templates for all DOMs in the detector. The new templates, shown in Figure 7.24, predict more hits with low charges, as observed in the 2015 data of Figure 7.23.

These new simulation SPE template are newly implemented in the iceCube simulation. Due to time constraints, the updated simulation has not been evaluated in the GRECO sample. In order to reduce the potential disagreement arising between data and simulation due to mismodeled low charges, both the data and simulation have been processed with a version of the Pegleg reconstruction designed to limit the dependence on charge information.

7.8.2 Disagreement in PMT Simulation

While investigating charge variables related to the SPE template, additional disagreements were discovered in the PMT simulation. The first suspected cause of charge disagreements was erroneous splitting of the waveform during charge extraction.

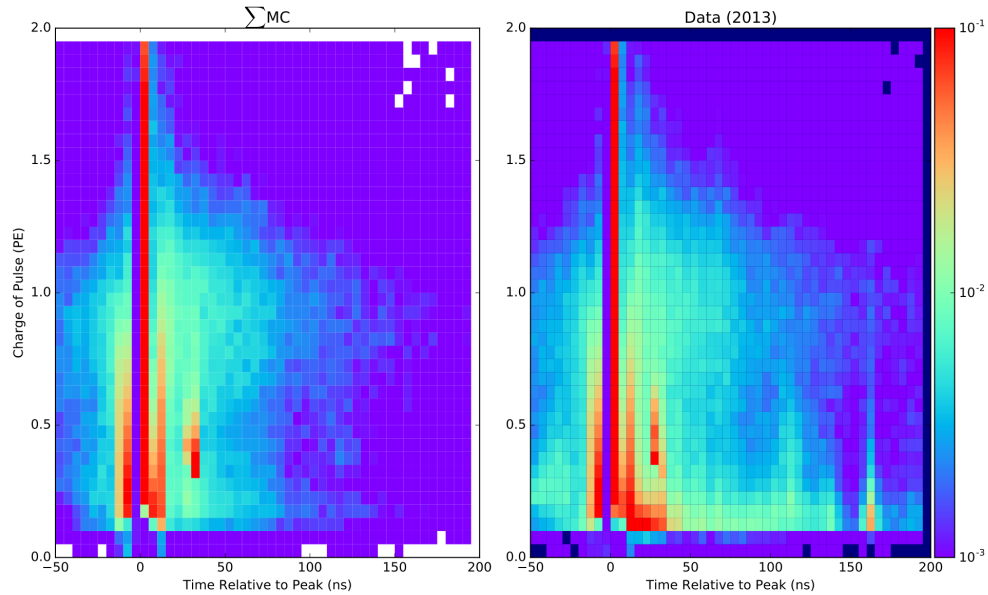


Figure 7.25 – A comparison of the charge extraction in data and simulation at GRECO L7. Both the time and charge are shown for individual pulses on all DOMs. The time is measured relative to the largest pulse observed on each DOM during an event. The data and simulation histograms are independently normalized to 1.0. While the two show broad agreement, notable differences occur at low charge.

The SPE template is used to convert the digitized waveforms from the FADC and ATWD into reconstructed photoelectrons consisting of charge and timing information. While the simulated response is known exactly when extracting pulses, the associated charge response of the DOM in data requires careful calibration. Using a mismodeled charge response to extract pulses in the data can result in single photoelectrons being erroneously split into multiple smaller reconstructed pulses.

Potential mismodeling effects of the charge extraction were checked in 7.25. In these figures, the charge of each individual pulse is shown as a function of the arrival time, which is normalized to the time of the largest extracted pulse in the DOM for each event.

Significant disagreements between the data and simulation are visible. The erroneously split pulses are visible in data as a low-charge tail from $t=0$ until $t=50$ nanoseconds. In addition to this effect, however, many other regions of disagreement are visible. In data, there appear to be a significant number of prepulses not visible in the simulation occurring between $t=-50$ and $t=-20$ nanoseconds. The structure of the late pulses, appearing with approximately 0.4 PE of charge and at time $t=30$ nanoseconds also appears notably different between the data and simulation. A final set of pulses, occurring at 160 nanoseconds, also appears to be unsimulated. This timing structure requires additional calibration resources to identify and better simulate, the scope of which is beyond this work. Regardless, the presence of unsimulated features indicates that at least some charge information in the simulation is unreliable.

The observed disagreements in the pulses and the SPE templates led to the removal of charge information from the Pegleg reconstruction. The disagreements remain unexplained, although updated calibration measurements may be performed using the GRECO sample. Using a procedure similar to that used for the fitting of the Vuvuzela

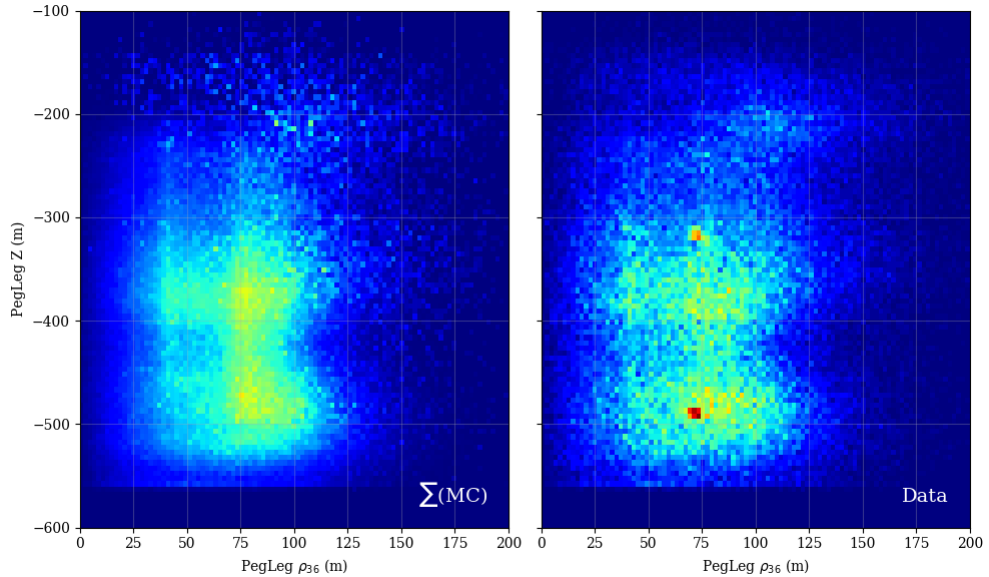


Figure 7.26 – The reconstructed Z position plotted against the reconstructed distance from string 36. The L7 cuts from GRECO have been removed for this plot. The colorbars in both plots have been normalized to be identical. The data and simulation show reasonable agreement except for two points in the data, near $\rho_{36} = 75$ at depths of -310 and -490.

V2 parameters (see Section 5.3), it may be possible to produce a more accurate model of the PMT effects in IceCube in the future.

7.8.3 Discovery of Flaring DOMs

Initial investigations into the poor agreement between data and Monte Carlo simulations led to comparisons of various reconstructed quantities believed to be independent of the expected signal. The decision was made to investigate these quantities using the simulation weights calculated with the baseline values.

Previous analyses have shown that the uncertainties in the ice model can lead to significant disagreements between data and simulation. The existing uncertainties on the bulk ice assume that the coefficients for all ice layers are fully correlated. However, it is possible that the ice model coefficients in parts of the detector are more poorly modeled than others. By looking at the event rate in data and simulation as a function of the depth and position in the detector, discrepancies in the ice model may be identified.

Two-dimensional histograms of the depth and radial distance also show systematic disagreement in some regions, as shown in 7.26. These excess events appear to occur on a single string, string 83, shown in 7.27, indicating an effect occurring due to the DOM hardware in the detector.

Follow-up work has shown that these DOMs, known here as *flaring DOMs*, appear to spontaneously emit light for unknown reasons. The light output is identifiable both based on the position of the hits and the amount of charge observed in nearby DOMs. These spurious events, first discovered in the GRECO selection, have since spawned dedicated searches to better understand spontaneous light emission from the DOMs. A small handful of DOMs have been identified by these searches with emission times as frequent as 1 Hz.

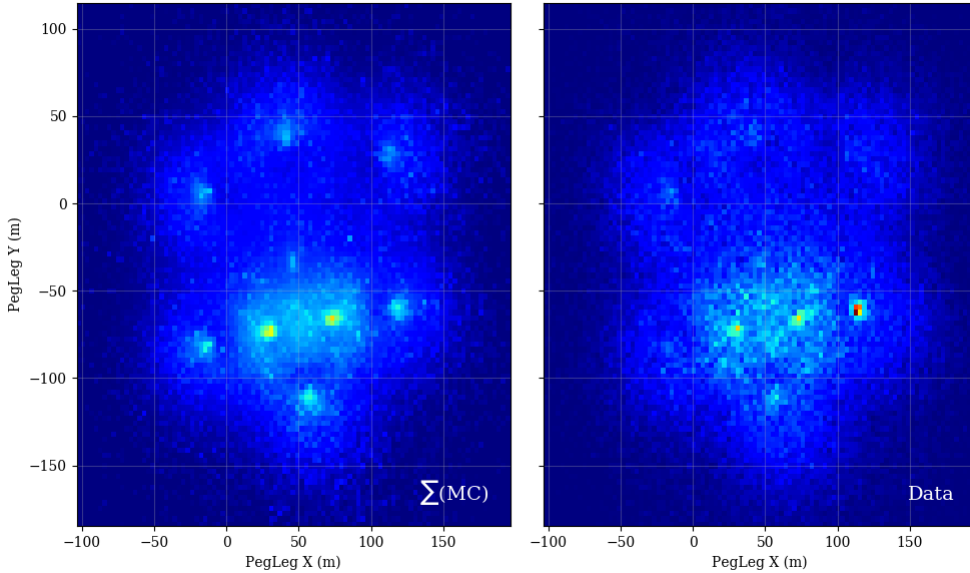


Figure 7.27 – The reconstructed X position and Y position of events in the detector. The L7 cuts from GRECO have been removed for this plot. The colorbars in both plots have been normalized to be identical. Once again, reasonable agreement is observed in most regions, although data events have a clear excess near $x=110$ m, $y=-60$ m. This position corresponds to string 83.

The affected events may be identified based on the charge profiles. DOMs directly adjacent to the emitting DOM observe a significant fraction of the total charge of the event. This may be characterized using the ‘charge RMS’ of the event

$$q_{RMS} = \frac{\sigma_q}{\sum_{hits} q_i} \quad (7.15)$$

This is shown in Figure 7.28. Events with a $q_{RMS} > 0.85$ are removed from the analysis, removing the most obvious spurious events. A total of 975 events are removed from the GRECO data, resulting in a total reduction of 1.3% of the event sample. The removal of these events in data and simulation does not significantly impact the sample due to the low event rates involved.

7.8.4 Simulation of Bedrock

Further investigations of the reconstructed Z position from Pegleg uncovered disagreements, shown in 7.29. A small deficit of events in data is observed at $Z \approx -450$. Checks performed with other samples have shown similar disagreements at these depths, indicating disagreement in the ice model. Previously unblinded oscillation samples showing this issue have not observed significant issues in the goodness-of-fit. New ice models are underway with dedicated work to fix this region is underway.

Near the bottom of the detector, a clear excess of events in data indicated a mismodeling in the simulation. Events which interact below the detector typically require higher energies than those inside the fiducial volume in order to trigger DeepCore.

In the GRECO selection, events with energies above 1 TeV are modeled using NuGen simulation in order to account for events not properly simulated in the GENIE generator. Previous investigations have shown that the two generators use similar models of the cross-section and return similar event rates at low levels. The events from the NuGen

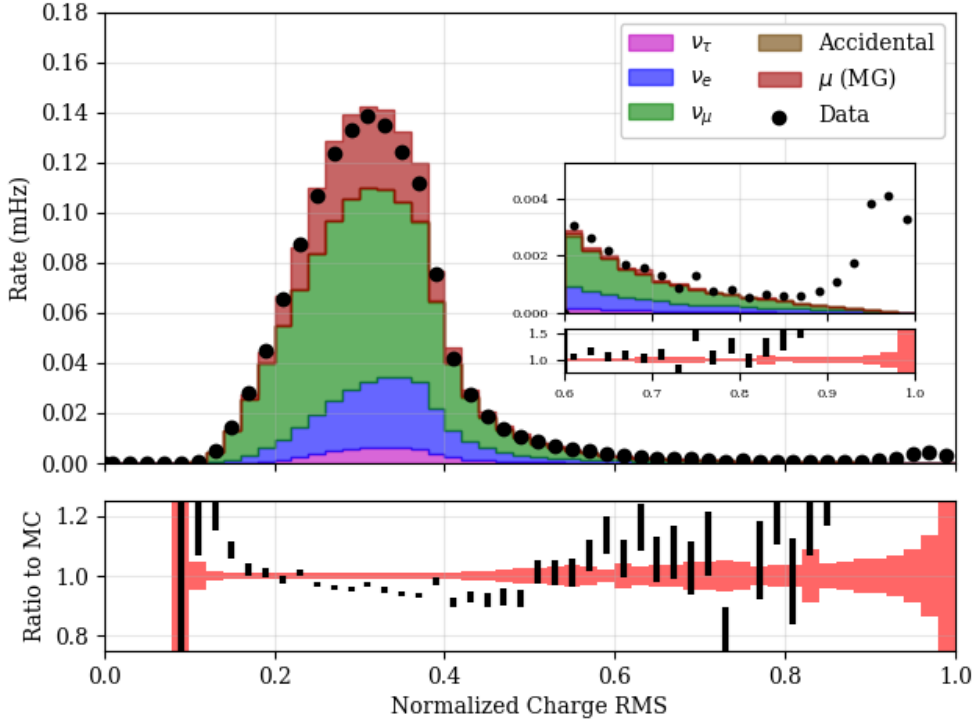


Figure 7.28 – The RMS of the charges within each event at final level. The value of the RMS is normalized using the total charge observed. The events with flaring DOMs cluster at high values of the charge RMS, visible in the inset.

generator were shown to make up a significant fraction of the high energy tail in the GRECO sample. These events were therefore checked for potential issues.

The NuGen and GENIE simulated event samples are merged in the GRECO analyses after removing NuGen events in overlapping energy ranges. The generated samples do include these overlapping regions, however. For the purposes of testing, the full sample of GENIE and NuGen events were compared in true and reconstructed energy and Z position. A comparison of the overlapping energy range of NuGen and GENIE events contained within the DeepCore fiducial volume showed some disagreement in the muon neutrino event sample. Figure 7.30 shows no disagreement in the neutral current and electron neutrino charged current events, indicating an effect specific to the muon neutrinos.

Limiting the energy range of both samples to the overlapping region 100-1000 GeV, other distributions may be checked. The cause of the discrepancy between the generators is shown in Figure 7.31. The two generators show broad agreement until a depth of approximately -830 meters, corresponding to the interface between the Antarctic glacier and the underlying bedrock. In the GRECO selection, only events with an outgoing muon have the range necessary to reach DeepCore from the bedrock.

Further checks discovered the issue in IceCube's implementation of the GENIE generator. When calculating the interaction probability for the neutrino interactions, the density of material is included. In the implementation of GENIE previously used by the IceCube collaboration, events were assumed to occur solely within or near the fiducial volume of DeepCore due to the low energies involved. The bedrock was therefore deemed unnecessary and not implemented in favor of assuming a uniform density of ice throughout the simulation volume. During initial implementation, the GENIE generator was planned

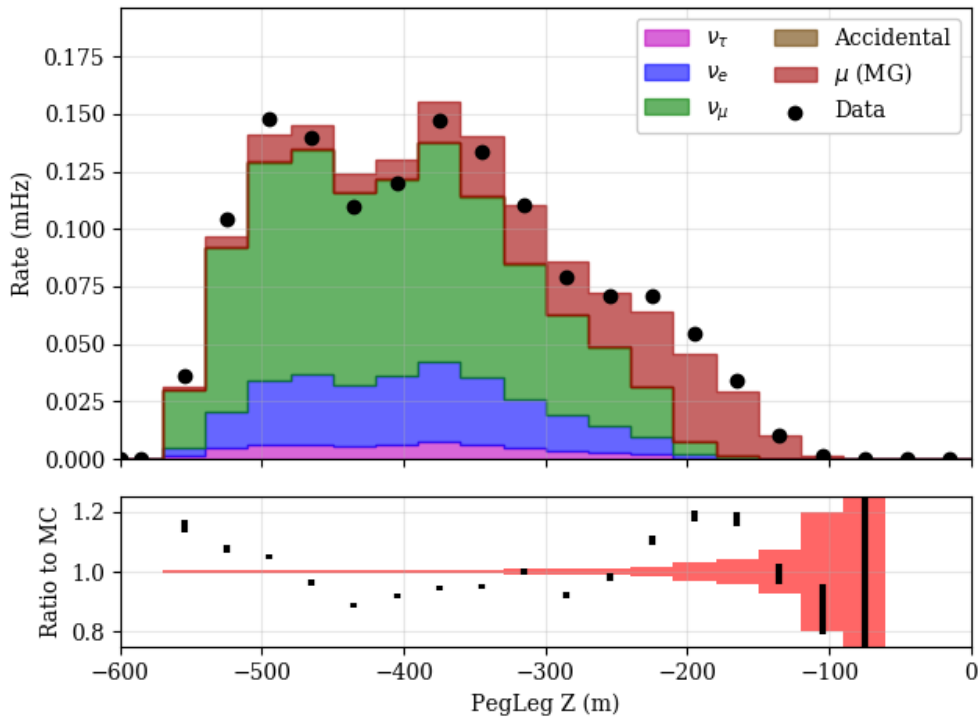


Figure 7.29 – The reconstructed Z position using PegLeg. The GRECO L7 cuts have not been applied in order to show discrepancies below the detector. Noticeable disagreement is seen below the detector at a depth of -500 m. Additional disagreements are also visible at the top of DeepCore, a region dominated by atmospheric muons.

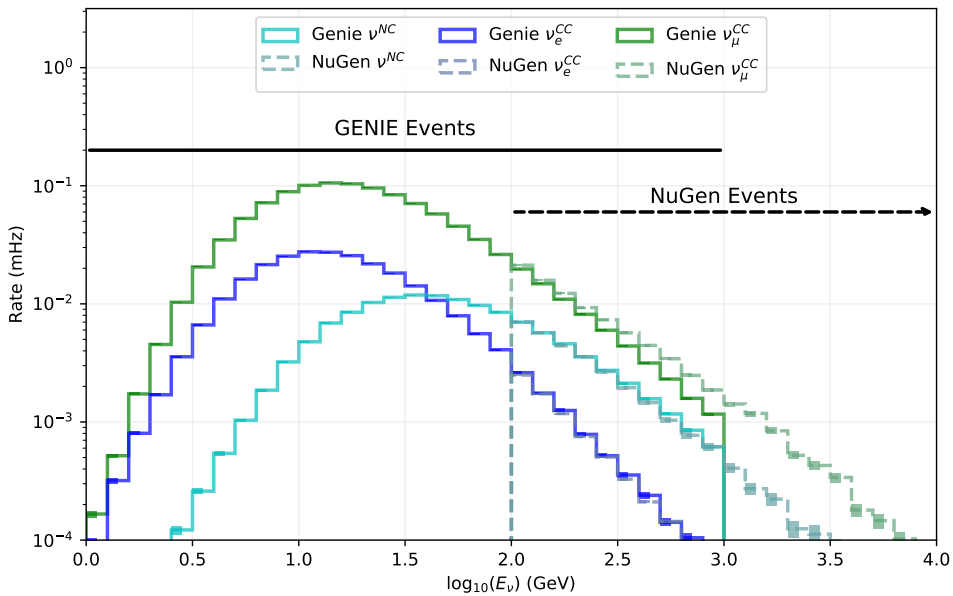


Figure 7.30 – The NuGen and GENIE true energy spectra at final level. The neutrinos are shown without oscillations applied. The overlapping energy range, 100-1000 GeV, show good agreement between the two generators for neutral current and electron neutrino charged current interactions. The muon neutrinos disagree in the overlapping energy range.

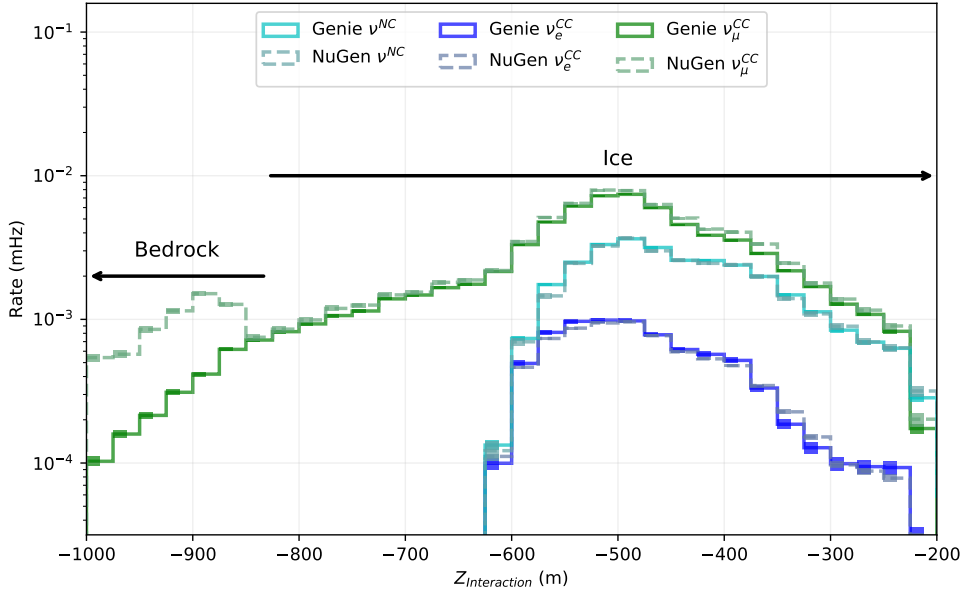


Figure 7.31 – The NuGen and GENIE interaction depths at final level. NuGen and GENIE agree above -830 m. The implementation of the GENIE generator in IceCube does not correctly model the bedrock at $Z < -830$ m.

for use up to 100 GeV due to technical limitations. Later work expanded this range up to 1 TeV with future work ongoing to push toward 10 TeV. The problems with the bedrock were mistakenly overlooked during the upgrades of the generator, leading to the systematic disagreement shown in Figure 7.29.

The bedrock has been properly included in both the NuGen generator as well as the PROPOSAL module for propagating the charged leptons. GENIE events therefore suffer solely from an incorrect interaction probability due to the discovered bug.

In order to limit other potential issues from the bedrock, the analysis space was restricted, removing events below the bottom of the detector ($Z_{reco} \leq -500$). This cut significantly reduces the size of the sample by reducing the high energy events included at final level. The additional cut has some impact on the expected sensitivity, but was deemed necessary to minimize the potential impact of systematics issues associated with the bedrock events.

7.8.5 Anisotropy of DeepCore

The reconstructed zenith and energy are used in the search for appearance. The azimuthal direction is not used for oscillation searches, but was checked for agreement.

As described in Section 3.2.2, the anisotropy of the ice model can bias the propagation of light in the detector in the azimuthal direction. This can result in azimuthally biased reconstructions. The anisotropy is characterized using a direction and magnitude, both of which are used to model the effect throughout the detector. The IceCube simulation assumes that the anisotropy is independent of depth.

The reconstructed azimuthal directions from Pegleg in the GRECO sample is shown in Figure 7.32. Both data and the simulated events show sinusoidal variation as a function of azimuthal direction, a result of the anisotropy in the ice. The effect in data is stronger than in simulation, indicating that the average anisotropy of the DeepCore fiducial region is stronger than assumed for DeepCore.

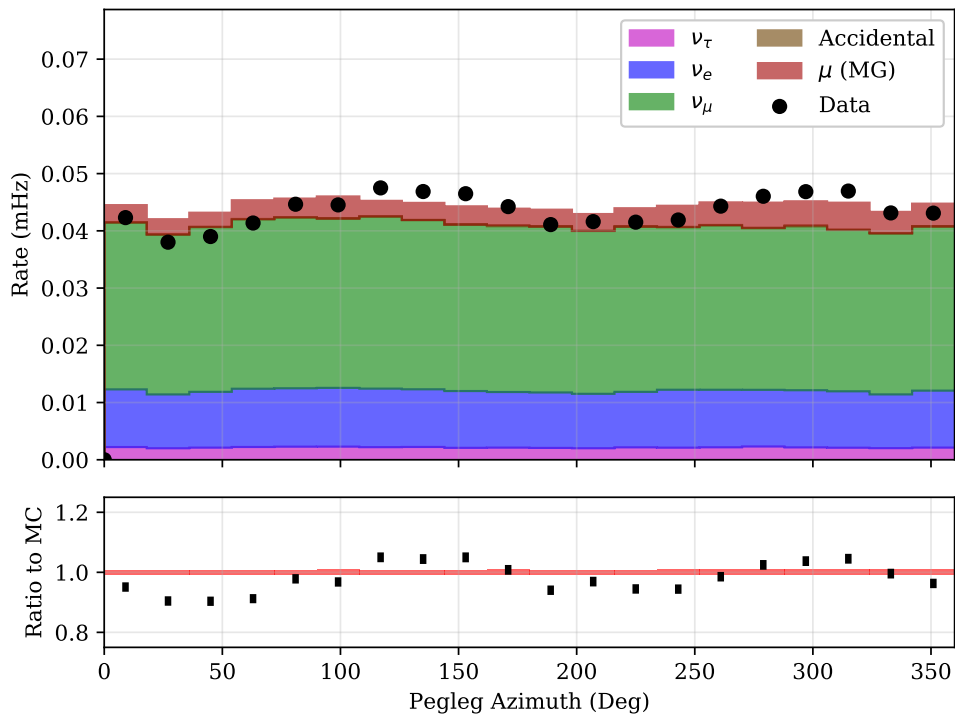


Figure 7.32 – The reconstructed azimuthal direction from the Pegleg reconstruction at GRECO Level 7. The data and simulation have been scaled to the same rate. A variation as a function of azimuthal angle is seen in both the simulated events and data, although the effect is stronger in data.

Type	IceCube Processing			GRECO				Analysis Binning
	Any Filter	DC Filter	Low-en L3	L4	L5	L6	L7	
CORSIKA	990598	9178	969.818	50.511	4.100	0.443	0.100	0.092
MuonGun	60669	2982	442.493	33.562	3.022	0.315	0.080	0.07
Accidentals	35855	8117	283.559	11.963	1.799	0.102	0.002	0.001
ν_e	1.842	1.721	1.262	0.783	0.544	0.362	0.325	0.194
ν_μ	11.317	6.360	4.758	2.503	1.629	1.011	0.676	0.552
ν_τ	0.293	0.270	0.206	0.134	0.103	0.074	0.051	0.045
MC Total*	1026466	17303	1260	65.893	8.176	1.991	1.153	0.884
Data	1154426	19092	1092	68.592	7.422	1.841	0.871	0.715

Table 7.8 – The event rates at each cut level in the GRECO selection. Note that the MuonGun events are included in this table, but do not contribute to the total Monte Carlo expectation to prevent double-counting of muon events from the CORSIKA sample. All rates are given in millihertz.

Figure 7.33 – The true neutrino energy and zenith of the GRECO sample at final level. The sample shows an asymmetry between upgoing ($\cos(\theta) < 0$) and downgoing ($\cos(\theta) > 0$) event rates in the neutrinos due to selection bias. The sample has a long tail of events at both high and low energies. Using the NuFit 2.2 oscillation parameters and the flux model from Honda, the ν_τ events are observed in the very upgoing region around $10^{1.4} = 25$ GeV.

The anisotropy effects of GRECO are the first hint that the anisotropy of the ice may not be uniform throughout the detector volume. New calibration measurements to incorporate these new properties into the simulation are underway. Because the anisotropy is not expected to directly impact the oscillation analysis, no additional cuts are introduced to the sample.

7.9 The Properties of the GRECO Event Selection

The completion of cuts yields the completed GRECO event selection. The rates of each sample of simulation and data are shown numerically in 7.8 or graphically in ???. Also included is the analysis binning as described in 8.1 for reference.

7.9.1 Energy and Zenith Reach

The GRECO sample covers a wide range of energies, with some final level events possessing energies as low as 2 GeV or as high as 1 TeV. The bulk of the neutrino sample, shown in ??, occurs at the expected oscillation minimum near 25 GeV. Most neutrino events originate at the horizon, as expected from the atmospheric neutrino flux, although there exists an asymmetry between the upward- and downward-going events. This asymmetry originates from the event selection, which selects against downward-going events in order to minimize the atmospheric muon background.

7.9.2 Reconstructed Variables

The true variables of the neutrino distributions are not observables in most GRECO analyses. Instead, all events are described using the reconstructed energies and zenith angles. The ν_τ sample reconstructs to slightly lower energies due to the loss in energy from the outgoing neutrino. The sample, when compared to data, shows reasonable

Figure 7.34 – The reconstructed energy and zenith of the GRECO sample at final level. Events in data reconstruct to both relatively high energies ($E_R > 100$ GeV) and very low energies ($E_R \approx 2$ GeV). Using the NuFit 2.2 oscillation parameters and the flux model from Honda, the ν_τ events are observed in the very upgoing region around $10^{1.4} = 25$ GeV.

shape agreement in both energy and zenith, although systematic disagreements occur above 100 GeV.

Something in here about resolution, you nitwit!

Bibliography

- [1] M. J. Larson. “Simulation and identification of non-Poissonian noise triggers in the IceCube neutrino detector”. M.Sc. Alabama U., 2013 (cit. on pp. 57–59, 78, 79).
- [2] K. A. Olive et al. “Review of Particle Physics”. In: *Chin. Phys. C38* (2014), p. 090001 (cit. on p. 57).
- [3] iminuit team. *iminuit – A Python interface to Minuit* (cit. on p. 63).
- [4] F. James and M. Roos. “Minuit – a system for function minimization and analysis of the parameter errors and correlations”. In: *Computer Physics Communications* 10 (Dec. 1975), pp. 343–367 (cit. on p. 63).
- [5] Joerg R. Hoerandel. “On the knee in the energy spectrum of cosmic rays”. In: *Astropart. Phys.* 19 (2003), pp. 193–220. arXiv: [astro-ph/0210453 \[astro-ph\]](#) (cit. on p. 65).
- [6] IceCube Collaboration, M. G. Aartsen, R. Abbasi, et al. “The IceCube Neutrino Observatory Part VI: Ice Properties, Reconstruction and Future Developments”. In: *ArXiv e-prints* (Sept. 2013). arXiv: [1309.7010 \[astro-ph.HE\]](#) (cit. on p. 65).
- [7] M. G. Aartsen, R. Abbasi, Y. Abdou, et al. “Measurement of Atmospheric Neutrino Oscillations with IceCube”. In: *Physical Review Letters* 111.8, 081801 (Aug. 2013), p. 081801. arXiv: [1305.3909 \[hep-ex\]](#) (cit. on pp. 70, 78).
- [8] IceCube Collaboration, M. G. Aartsen, M. Ackermann, et al. “Determining neutrino oscillation parameters from atmospheric muon neutrino disappearance with three years of IceCube DeepCore data”. In: *ArXiv e-prints* (Oct. 2014). arXiv: [1410.7227 \[hep-ex\]](#) (cit. on pp. 70, 78).
- [9] IceCube Collaboration, M. G. Aartsen, M. Ackermann, et al. “Measurement of Atmospheric Neutrino Oscillations at 6–56 GeV with IceCube DeepCore”. In: *ArXiv e-prints* (July 2017). arXiv: [1707.07081 \[hep-ex\]](#) (cit. on pp. 70, 78).
- [10] IceCube Collaboration, M. G. Aartsen, M. Ackermann, et al. “Search for sterile neutrino mixing using three years of IceCube DeepCore data”. In: *ArXiv e-prints* (Feb. 2017). arXiv: [1702.05160 \[hep-ex\]](#) (cit. on p. 70).
- [11] J. van Santen. “Neutrino Interactions in IceCube above 1 TeV: Constraints on Atmospheric Charmed-Meson Production and Investigation of the Astrophysical Neutrino Flux with 2 Years of IceCube Data taken 2010–2012”. PhD thesis. U. Wisconsin, Madison (main), 2014 (cit. on pp. 71, 90).
- [12] Eric Jones, Travis Oliphant, Pearu Peterson, et al. *SciPy: Open source scientific tools for Python*. [Online; accessed <today>]. 2001– (cit. on p. 74).
- [13] M. Leuermann. “Testing the Neutrino Mass Ordering with Three Years of IceCube/DeepCore Data”. Pending. Ph.D. URheinisch-Westfälische Technische Hochschule (RWTH), 2018 (cit. on pp. 75, 97, 99).

- [14] S. Schoenen. “Discovery and characterization of a diffuse astrophysical muon neutrino flux with the iceCube neutrino observatory”. Ph.D. Rheinisch-Westfälische Technische Hochschule (RWTH), 2017 (cit. on p. 75).
- [15] M. G. Aartsen, M. Ackermann, J. Adams, et al. “The IceCube Neutrino Observatory: instrumentation and online systems”. In: *Journal of Instrumentation* 12 (Mar. 2017), P03012. arXiv: 1612.05093 [astro-ph.IM] (cit. on p. 76).
- [16] R. Abbasi, Y. Abdou, T. Abu-Zayyad, et al. “The design and performance of IceCube DeepCore”. In: *Astroparticle Physics* 35 (May 2012), pp. 615–624. arXiv: 1109.6096 [astro-ph.IM] (cit. on pp. 78, 79).
- [17] S. Euler. “Observations of Oscillations of Atmospheric Neutrinos with the Ice-Cube Neutrino Observatory”. Ph.D. Rheinisch-Westfälische Technische Hochschule (RWTH), 2013 (cit. on pp. 78, 87, 95, 97).
- [18] Andreas Hocker et al. “TMVA - Toolkit for Multivariate Data Analysis”. In: *PoS ACAT* (2007), p. 040. arXiv: physics/0703039 [PHYSICS] (cit. on pp. 81, 84).
- [19] AMANDA Collaboration. “Muon track reconstruction and data selection techniques in AMANDA”. In: *Nuclear Instruments and Methods in Physics Research Section A: Accelerators, Spectrometers, Detectors and Associated Equipment* 524.1 (2004), pp. 169 –194 (cit. on p. 84).
- [20] D. Pandel. “Bestimmung von Wasser- und Detektorparametern und Rekonstruktion von Myonen bis 100 TeV mit dem Baikal Neutrino-Teleskop NT-72”. PhD thesis. Humboldt-Universität, 1996 (cit. on p. 90).
- [21] AMANDA Collaboration. “Muon track reconstruction and data selection techniques in AMANDA”. In: *Nuclear Instruments and Methods in Physics Research A* 524 (May 2004), pp. 169–194. eprint: astro-ph/0407044 (cit. on p. 90).
- [22] J. A. Nelder and R. Mead. “A Simplex Method for Function Minimization”. In: *The Computer Journal* 7.4 (1965), pp. 308–313. eprint: /oup/backfile/content_public/journal/comjnl/7/4/10.1093/comjnl/7.4.308/2/7-4-308.pdf (cit. on p. 90).
- [23] IceCube Collaboration, M. G. Aartsen, R. Abbasi, et al. “The IceCube Neutrino Observatory Part II: Atmospheric and Diffuse UHE Neutrino Searches of All Flavors”. In: *ArXiv e-prints* (Sept. 2013). arXiv: 1309.7003 [astro-ph.HE] (cit. on p. 92).
- [24] J. Kiryluk and for the IceCube Collaboration. “First search for extraterrestrial neutrino-induced cascades with IceCube”. In: *ArXiv e-prints* (Sept. 2009). arXiv: 0909.0989 [astro-ph.HE] (cit. on p. 92).
- [25] M. Dunkman. “Measurement of Atmospheric Muon Neutrino Disappearance with IceCube-DeepCore”. Ph.D. The Pennsylvania State University, 2015 (cit. on pp. 96, 97).
- [26] F. Feroz, M. P. Hobson, and M. Bridges. “MultiNest: an efficient and robust Bayesian inference tool for cosmology and particle physics”. In: *Monthly Notices of the Royal Astronomical Society* 398.4 (2009), pp. 1601–1614. eprint: /oup/backfile/content_public/journal/mnras/398/4/10.1111/j.1365-2966.2009.14548.x/2/mnras0398-1601.pdf (cit. on p. 99).
- [27] F. Feroz, M. P. Hobson, E. Cameron, and A. N. Pettitt. “Importance Nested Sampling and the MultiNest Algorithm”. In: *ArXiv e-prints* (June 2013). arXiv: 1306.2144 [astro-ph.IM] (cit. on p. 99).

-
- [28] M. G. Aartsen, R. Abbasi, M. Ackermann, et al. “Energy reconstruction methods in the IceCube neutrino telescope”. In: *Journal of Instrumentation* 9, P03009 (Mar. 2014), P03009. arXiv: 1311.4767 [physics.ins-det] (cit. on p. 99).
 - [29] Y. Hasegawa. *Analysis of Charge Response functions of the IceCube PMTs*. Chiba University. 2007. URL: <http://www.ppl.phys.chiba-u.jp/research/IceCube/pmt/SPE/CRAnalysis.html> (cit. on p. 104).

Notes

■ Add a plot of the oscillation probabilities here	31
■ find good quality swedish camera pics?	47
■ Something in here about resolution, you nitwit!	113
■ list of atmo disappearance measurements that use zenith and energy binning .	114
■ dragon, leesard 3 year papers	114
■ dragon, leesard	114
■ cumulative plot of track length	114
■ cumulative plot of deltallh	114
■ roc curves for track length	114
■ this sentence needs to be reworded. its too verbose	114
■ mc templates!	115
■ nufit 2.2	115
■ PDG	115
■ superk paper, opera paper sources for unoscillating NC	115
■ non-sterile explanations of non-unitarity? maybe the neutrino decay paper? .	116
■ think up a better phrasing to introduce the tau normalization	116
■ Crazy shit that I will probably take out. but maybe find the neutrino decay paper again?	116
■ opera tau neutrino event views	116
■ opera paper: https://arxiv.org/abs/1507.01417	116
■ superk paper on appearance https://arxiv.org/pdf/1711.09436.pdf	117
■ https://arxiv.org/pdf/1711.09436.pdf again	117
■ wtf is going on here? table 1 in the paper gives an expectation of 185.2 events, but the stuff at the top right of page 11 says the expectation is 224...?! and NIETHER of these give the 1.47 that they quote. wtf	117
■ figure 14 of https://arxiv.org/pdf/1711.09436.pdf	117
■ nufit 2.2	117
■ genie	118
■ coin fraction figure	121
■ Hammamatsu quantum efficiency? http://www.hamamatsu.com/resources/pdf/etd/LARGE_AREA_PMT TPMH1286E.pdf	121
■ How many were tested in a lab before deployment?	121
■ Where does the domeff prior come from?	121
■ domeff	121
■ ice model	121
■ bulk ice uncertainties vs depth	121
■ absorption	122
■ scattering	122
■ hole ice and hifwd	122

██████	how do i flesh this out?	123
███	muongun rates vs domeff and absorption to justify exponentials	123
██████	Need to include some discussion of th goodness of fit for these sets. Maybe a plot of the chi2 values for all of the sets?	123
███	chi2 values for hyperplane parametrizations	123
██████	This needs work. can't even be called a derivation. its just crap.	123
███	make a plot showing chi2 value as a function of mc stats scale factor to justify the 10x rule	124
██████	this is only true for muons! how do i explain that?	124
███	All of these references for the priors...	125
██████	Maybe all of this oscfit stuff should just be moved to just before the systematics section.	127
██████	should i even talk about oscfit itself? it seems a bit awkward	127
███	msu and desy disappearance	127
███	Flowchart of oscfit fitting. at least broadly	127
███	prob3++	127
███	nufit 2.2	127
███	iminuit	127
███	asimov expectation?	128
███	asimov sensitivity	128
███	brazilian flag	129
███	comparison of stat-only fit to full systematics fit	132
███	N+1 tests	132
███	N-1 tests	133
███	hidden potential martin n-1 tests	133
███	should i be including the dropped dis/theta13 systematics here? and maybe deltacp? otherwise this section feels a bit pointless	133
███	may just remove the burn sample crap. its so out of date that its too weird to go back and redo it.	133
██████	blahdy blahdy blahdy. no point spending time here if i may just kill it	133
███	scipy	134
███	PDFs for gof	134
███	future reference to martin, elim's theses	138
███	elim's thesis	138
███	iminuit	138
███	elim's result!	138
███	icecube 2017 result	138
███	superk 2015 oscillation result	138
███	minos oscillation with atm	138
███	nova oscillation	138
███	t2k oscillation result	138
███	nufit 3.2	138
███	martin's thesis	138
███	martin's kdes from the aachen group. who did that?	138
███	pingu paper and/or pisa paper describing nmo measurement	139
███	Need martin's final result!	139
███	chi2 scans of the detector systematics to show greco constraints on domeff, holeice, hifwd, absorption, and scattering	139
██████	change cc and nc+cc to exclusive and inclusive respectively?	139

 superk result	139
 opera result	139
 what's the livetime increase from loosing the GRL?	140
 check the run dates	140